POLITECNICO
MILANO 1863

SCUOLA DI INGEGNERIA INDUSTRIALE
E DELL'INFORMAZIONE

Photovoltaic Power Reduction: Degradation effects on system output and Model Based Algorithm validation and maintenance

TESI DI LAUREA MAGISTRALE IN
ELECTRICAL ENGINEERING-INGEGNERIA ELETTRICA

Author: **Monica Valeria Cattaneo**

Student ID:	10469625
Advisor:	Loredana Cristaldi
Co-advisor:	Christian Laurano
Academic Year:	2021-22

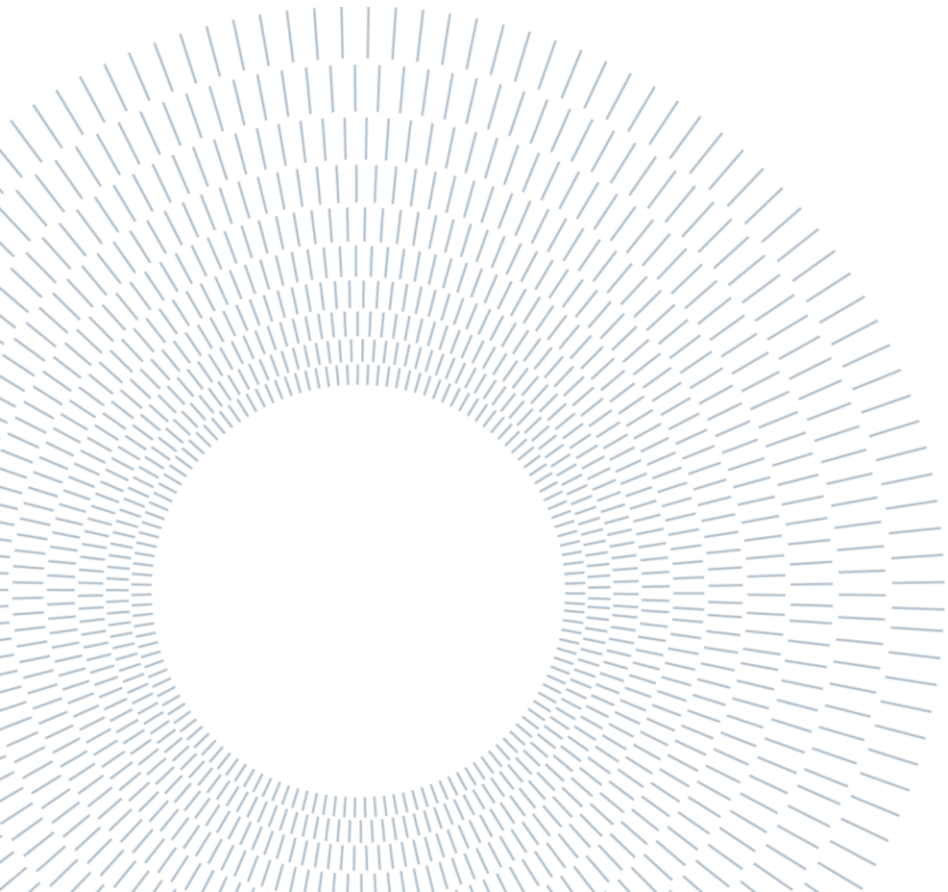

Abstract

Reliability research on photovoltaic modules is still underdeveloped. Factors and modes involved in decreasing system performance are studied. They depend on environmental conditions, technology, design and materials used. It is essential therefore, a detailed study on these factors to then be able to quantify module' degrade. In literature there is a wide collection of studies aimed to solve the problem. It is necessary to understand the multiplicity dependance, it is quite difficult to define an accurate model which comprehend all modes. At the same time, given the increased permeability from renewable sources, RES, a control system able to reduce power output of the PV system will aid frequency regulation. This elaborate is an attempt to optimize the algorithm reducing its dependency on data error. The data is previously filtered by noise, partial shading and interpolation error due to values of current and voltage at maximum power point. Then an error study is performed between model output and interpolation result scaled by a reduction percentage, before and after constraints. The error was then statistically analyzed to understand if it respects the tolerance limits defined in European and national normative.

Key-words: degradation modes, PV reliability models, power reduction control strategies, frequency regulation, data analysis.

Abstract in lingua italiana

La ricerca sull'affidabilità dei moduli fotovoltaici è ancora poco sviluppata. Si sono ricercati i fattori e le modalità che intercorrono a ridurre le performance di sistema. Essi dipendono da condizioni ambientali, tecnologia, design e materiali usati nel realizzarli. È perciò imprescindibile uno studio dettagliato su questi elementi per poi riuscire a quantificare il degrado del pannello. In letteratura si trovano molti studi versi a solvere questo problema. C'è però da comprendere che, vista la molteplice dipendenza, è alquanto complesso definire un modello che accuratamente li comprenda tutti. Parallelamente, data la crescente permeabilità del mercato energetico da fonti rinnovabili, RES, si è proseguita la ricerca su un sistema di controllo della potenza in uscita per far fronte alla regolazione di frequenza. In particolare, forniti un database di dati riguardanti un modulo e l'algoritmo, si è cercato di ottimizzarlo riducendo la sua dipendenza da errori di dati. In primo i dati, precedentemente filtrati da rumore di misura, sono stati ulteriormente filtrati da partial shading ed errori di interpolazione legati al calcolo dei valori di corrente e tensione nel punto di massimo di potenza del modello. In secondo si è calcolato l'errore tra l'output di modello e il risultato dell'interpolatore, scalato dalla percentuale, prima e dopo il filtraggio. L'errore è stato statisticamente analizzato per capire se rientra nei limiti definiti dalla normativa nazionale ed europea.

Parole chiave: modalità di degrado, modelli di affidabilità per PV, strategie di controllo per riduzione di potenza, regolazione in frequenza, analisi dati.

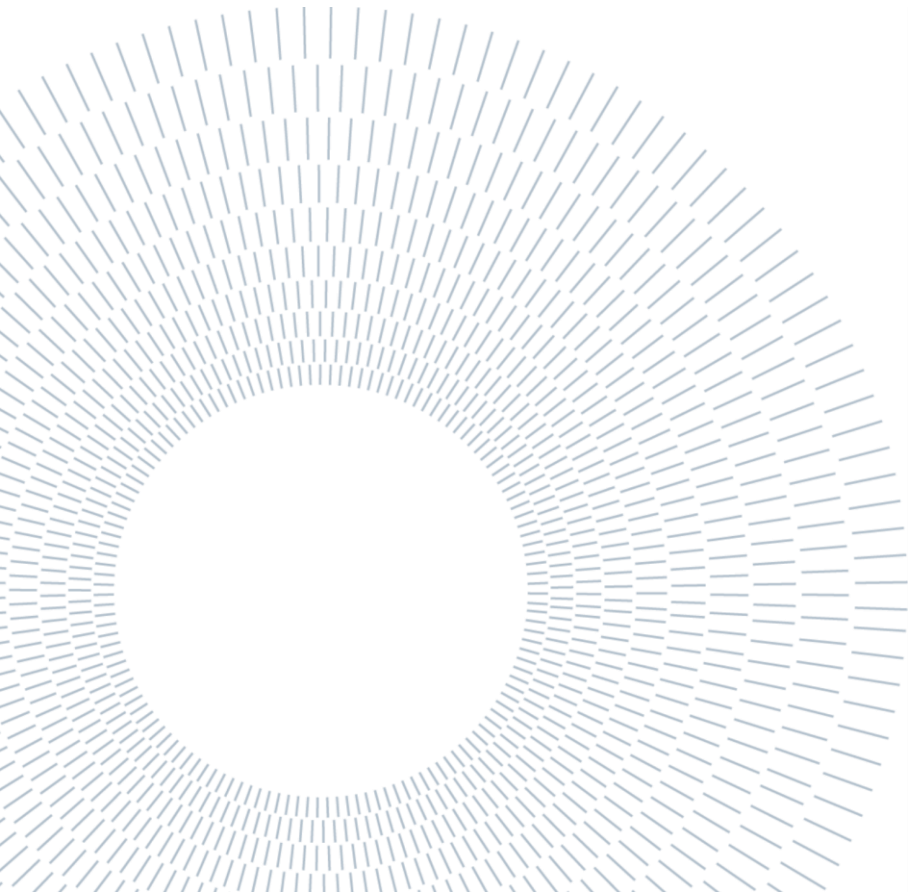

Contents

Introduction

Photovoltaic is one of the most important and promising renewable energy sources along with wind generation. With its installed capacity growing due to decrease of cost production and state incentives, solar systems can be found in many forms, as power generation stations, at distribution level with residential systems or isolated systems and as low power chargers. But although its use has become established and public consensus is generally positive with the rising awareness of green solutions implementation to break away from highly pollutant, scarce and geographically unevenly distributed traditional fuels, oil and carbon, this technology faces many challenges.

The energy source is sunlight, present everywhere but only during daytime. Since the source is intermittent and not constant as it is conditioned by many variables, location and weather conditions, it needs a backup to provide continuously electric energy to the loads. Weather conditions are factors leading to the system degradation in time, they act combined with intrinsic manufacturing defects and bad handling of the panel. Power degradation is a power reduction which cannot be reversed, and it is important to be studied so to quantify it and assure the reliability of the PV panel.

Another issue is low efficiency, though in the years technology improvements are rising this value. The low efficiency forces system operators to work the PV plant at maximum power point in order to optimize and get the maximum power output out the system. But as the grid is a network highly connected with several and diverse kind of power generators ancillary services, previously provided by traditional generators, are undermined. A blatant example is frequency regulation. Usually, rotating machine inertia contributes to stabilize frequency drop and rise but a grid with permeated photovoltaic systems may not be able to face this problem. Thus, a power control on solar system can involve PV system in this service. The task of the control is to reserve a certain amount of power to solve the frequency issue, and this is done working away from the maximum power point, so at reduced power.

This thesis aim is to study power reduction of a photovoltaic system. Power reduction can be linked to unwanted causes like degradation of power output with permanent effect on the module performance or can be operated to implement further functions,

aside from power generation, able to help the interconnected system to the PV as in case of frequency regulation with PV systems participation.

This elaborate is structured in the following way; in *Chapter 1* a brief introduction to the photovoltaic module structure, functioning and materials is done in order to anticipate important concepts useful to understand other chapters content, in *Chapter 2* degradation literature review research is performed with focus on degradation models which could be applied to predict photovoltaic power output, in *Chapter 3* the issue of frequency regulation is introduced along the PV participation to the problem and finally in *Chapter 4* a power reduction algorithm is presented.

Abbreviations

AC	Alternate current
AF	Accelerated Factor
APC	Active Power Control
AT	Accelerated Test
BESS	Battery Energy Storage System
BO	Boron Oxygen
CPG	Constant Power Control
DC	Direct current
DH	Damp Heat
DPC	Delta Power Control
ESS	Energy Storage System
EVA	Ethylene Vinyl Acetate
FF	Fill Factor
IEC	Commission Électrotechnique Internationale (International Electrotechnical Commission)
LID	Light Induced Degradation
MPP	Maximum Power Point
OLS	Ordinary Least Square

PID	Potential Induced Degradation
PV	Photovoltaic
RH	Relative humidity
STC	Standard Test Conditions
T	Temperature
UV	Ultraviolet
YI	Yellowness Index

1. Focus on PV

In this chapter the basic knowledge on photovoltaic will be briefly reviewed. From the operating principle which enable energy conversion and power production to the module structure and the composing materials.

1.1 Operating Principle

The purpose of Photovoltaic (PV) technology is to convert sunlight energy into usable electrical energy. This is the photovoltaic effect.

When light reaches the PV cell surface electrons inside the silicon wafer are energized and are able to jump from the bottom layer to the top, crossing the gap band of the p-n junction, producing a voltage. This voltage, photovoltage, drives a current. The DC current is later converted into AC and fed to the load.

All of this is possible due to the material used in PV cell: silicon. Chemically silicon possesses fourteen electrons (negative charges) among which four can be shared or donated (valence electrons). This means that they are loosely bound to the atom and when an appropriate amount of energy, as it is light under certain conditions, is fed it can 'free' the electrons. Unbounded electrons move inside the silicon crystal leaving behind a 'hole' which can be occupied by another roaming electron. But this alone does not produce any current or voltage. The photovoltaic effect exists only if a potential barrier is present. It is like a line between the p-type cell and the n-type cell, see Figure (1.1-1), where holes stay into p-cell and electrons pass into the n-cell. Electrons are collected by a metallic grid.

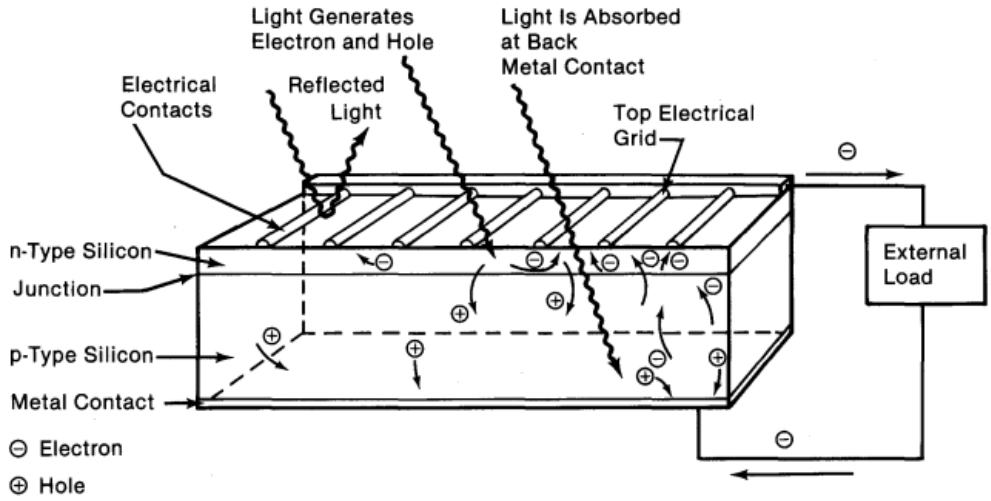

Figure 1.1-1 Photovoltaic effect scheme [1]

1.2 Materials and Structure

PV panel is a modular and multi-layer structure which may include connections to an electrical system, each layer, Figure (1.2-1) has a precise purpose. Modularity consent to have high values of current and voltage and consequently more power produced.

-PV cells and metallic print

-Encapsulant

-Outer covering: front and back

-Frame

-Junction box

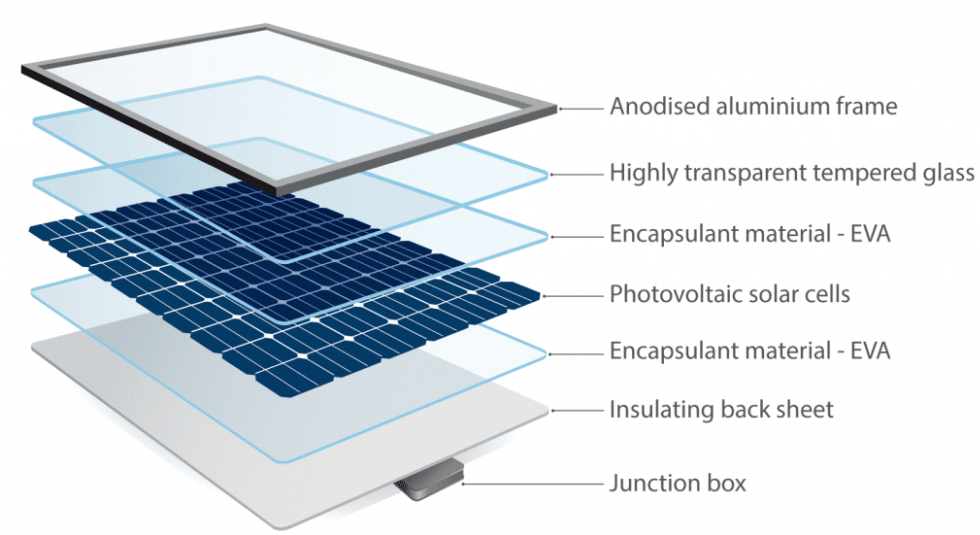

Figure 1.2-1 PV module structure extrusion [Figure from Recycling Solar Panels - GSES]

1.2.1 PV cells and metallic print

The key element of a PV module is silicon, SiO_2, a wide available mineral. This mineral is processed in an arc furnace to obtain a pure form of silicon; SiO_2 is heated with carbon at 1900°C, the high temperature enables the oxygen to split from silicon and bond with carbon resulting in CO_2 (carbon dioxide) and CO (carbon monoxide). Then, through the Czochralski process silicon crystals are obtained; the furnace product is liquefied in a tank and the seed crystal is introduced hanging on a wire, the wire is rotated, while being doped, and slowly the crystal begins to grow, after a few days the process is completed. Each ingot is shaped to have the same size and sliced in thin paper of thickness 100-500 μm. Each cell is pre-processed with an anti-reflective coating (ARC) to maximize irradiation absorption (the less is reflected the more power is produced) this is because bare silicon can reflect more than 30% of sunlight; the ARC is a dielectric of opportune thickness which drastically reduce the percentage of reflected light in a certain wavelength range.

There are two types of solar cells, p-type and n-type. Solar panels were firstly used in space, the p-type, as they were quite robust and resistant to space irradiation, they are doped with boron which has one electron less than silicon, hence the cell is positive. The same technology was implemented on Earth but with quite different results so n-type cells are indicated for earth application as they are immune to boron-oxygen defects (BO), as they are doped with phosphorus which has one electron more than

silicon making the cell negative. The BO is caused by oxygen absorbed during the ingot formation; it interacts with boron leading to a severe loss of performance only in the first hours of exposure to light. The n-type is efficient and not affected by light induced degradation (LID) thanks to its neutrality from the boron-oxygen defect. Both cells are used (though p-type is more diffuse due to historical reasons). To avoid such defect the p-type cells are passivated with additives meaning that it won't get activated when the panel is switched on but, as modules are placed in open field, external factors could activate this defect (mostly temperature).

To draw current, cumulation of negative charges, small rectangles of metal are placed on top of the cell, the busbars, along with perpendicular metallic wires, the fingers. Fingers conduct electrons to the busbar which conducts the DC current to the junction box sealed on the back of the panel. Both fingers and busbars are screen printed on the front of the solar cell. They are made of conductive materials, usually copper coated with silver or tin. The coating enhances conductivity and lower oxidation under normal operating condition. The current can also be drawn through the back metallic surface.

Cells are connected in series with tab wires, to increase the voltage and in parallel with bus wire, to increase the current. Groups of cells form a module, connected modules constitute a panel and a panel assembly is called solar array. The modularity is quite convenient as it permits to have desired of voltage and current. But, at the same time, high levels of voltage can be a risk to safety.

1.2.2 Encapsulant

The first layer around the cells is the protective sheets of polymer applied to the front and back of the cell composition, they made sure to offer mechanical strength, avoid harming UV rays reaching the cells (UV rays spectrum range is not used by cells in most application), maintain optical transmittance, maintain physical isolation from environment factors such rain and humidity, maintain electrical insulation and electrical integrity of the electric circuit. The most common encapsulant is Ethylene-vinyl acetate (EVA); a thermoplastic polymer made by ethylene and vinyl acetate (from 10-40%), it is flexible, soft and possesses optical transparency.

But over time this material due to the acetate component and UV effect gets discolored, from transparent the color changes first to yellow and then, in extreme cases, to brown; visibly reducing the light transmittance from sun to cells reducing cell efficiency. The reaction taking place is due to a hydrolysis phenomenon caused by water vapor, this results in acid formation which corrodes metal contacts and creates bubbles. Due to these problems in the long-term life of modules EVA encapsulant needs to be

improved or alternatively new materials research has to be done. Incorporating additives can be a good solution if the purpose is to enhance a specific property of EVA but it always comes with a trade-off, where some improvements are reached and new disadvantages could rise. Aside its composition the main problems in encapsulant derives from the lamination process. This process subjects the module composing layers to high temperature and pressure in order to: remove air, remove humidity and melt the encapsulant homogeneously on cells surface. A wrong lamination could lead to loss of additives with consequent loss of adhesion, the 'pinch-out' lead to stress on the edges of the module where pinches clamp the composition reducing the encapsulant thickness with delamination effect.

1.2.3 Outer Covering: front glass and back sheet layer

To further protect the solar module aside from the encapsulant other layers are needed; the front and the back layer. The choice of materials depends on the kind of application. The 'traditional' solar panel front layer is constituted by glass while the back is made of foil (laminated PV modules); in some cases, also the back is made of glass. The front glass which protects the module is tempered to resist breakage and possess excellent transparency (up to 92%). The thickness ranges from 2 to 4 mm. Glass breaking are due to thermal shocks or heavy loads like hail of important size. Some glasses present a pattern which increase the amount of light trapped yet increases the possibility of dust and dirt deposit. Breakage is also due to the 'pinch-out'.

1.2.4 Frame

The frame joins all layers together, it is made of aluminum, a light metal. As any metal it can conduct electricity, that's why an appropriate sealing is needed in order to avoid any external substance ingress, particularly moisture. The frame must perfectly fit the layers sandwich, wrong measures could compress the composition leading to cell and glass crack, or it may come loose and let humidity in. The frame must be correctly grounded to avoid electrical risks.

1.2.5 Junction box

It is an intermediate element which brings outside the electrical connections. Inside this box there are protective by-pass diodes which allow the current to flow strictly one way and allow energy production even if a cell is shaded. The junction box sealing shall not let water in to avoid electrical risk in case of connectors contact.

1.3 conclusion

This brief introduction on PV manufacturing and materials can give some hints to the criticality when dealing with PV technology:

- Boron-oxygen defects
- By pass diodes
- Lamination process
- Small wafer thickness
- Sealing issue
- Modularity

2. Degradation Models-A Literature Review

The previous chapter 'Focusing on PV' gives an idea on the main criticalities when dealing with solar panels. The choice of materials from the cell to the layers which protect the module, the manufacturing process and situ installation influence the lifetime of these energy converters. The question is how much?

To answer this question in this chapter literature research on degradation models is done. But before it will be illustrated all the steps leading to degradation and the difficulties of this area of research. The main modes will be explained alongside models. Dealing finally, with effects on power performance.

2.1 Qualification and Quantification Tests

Since photovoltaic modules were used in terrestrial applications, degradation was a concerning matter as Earth's atmosphere and space differs. The surrounding environment influences the life of the module. Outdoor applications subject the PV module to environmental stresses. These factors lead to failure modes, unwanted effects in the panel able to lower PV performance, some reversible and other permanent.

Up to date there are no official approved reliability tests concerning photovoltaic technology [1]. Reliability tests evaluate failures, quantify them and understand the reason behind them so to improve reliability.

The present normative related to photovoltaic does not give any sort of quantitative metric to evaluate the panel performance, just qualitative under the standard IEC 61215. Qualitative tests are just pass or fail tests and are useful to minimize infant mortality [1, 4]. But what is the difference between Qualitative and Quantitative tests and what their purpose? In [9] the following definitions are given: "*A Quantitative AT tests units at combinations of higher than-usual levels of certain accelerating variables. The*

purpose of a Quantitative AT is to obtain information about the failure-time distribution or degradation distribution at specified "use" levels of these variables" while "*A Qualitative AT tests units at higher-than-usual combinations of variables like temperature cycling and vibration…The purpose of such tests is to identify product weaknesses caused by flaws in the product's design or manufacturing process*".

From the above definitions it is easy to understand that module long lifespan makes output data collection burdensome, a module can last from 20 up to 30 years. For such reason accelerated tests are a good solution. They simulate environmental stresses for a period of time shorter than the module lifespan giving sufficient amount of data to be analyzed [1, 7]. But they also bring some disadvantages such as 'higher than usual levels' of environmental stresses which may not be encountered in field conditions. And usually, just a couple of accelerated factors can be applied to the tested module. Stress combination, more factual, is far realistic than just considering few factors.

Further concerns come from the effect of AF, modes. It can be that modes manifest on the module are different both in the kind of and their severity, in other cases some modes may never appear while some may happen but at a different time instant than when appearing under real conditions [1].

Reliability tests are Quantification tests, they will tell when the power output of the module will not be sufficient to keep the system on. Costs will be higher than revenues. Warranties tells that after 20-25 years the power reduction amounts to 20% without power tolerances and around 10% less with [1].

Photovoltaic research is evolving without having sufficient output data on how to improve the panel characteristics. Nor the data acquired is of recent technologies but old data of old PV plant installations. Degradation models are thus a necessary tool to increase trust in the PV technology. Both on the consumer and the investor side. The lifetime study of photovoltaic modules will quantify the module performance opening new doors to research on ways to improve the panel performance and reliability.

2.2 Modes

PV module technology possesses a long warranty period which spans over 25 years [1-2], this period is shared among manufacturers yet long period warranties do not mean the product is reliable, of course PV modules are highly reliable items but during their lifetime, failures can occur leading to a rapid deterioration of the module characteristics and to a permanent power loss especially in large grid connected power stations even though they may have passed qualification standards [2]. The possibilities of failure derive from its outdoor placement. It is necessary to better predict the PV system behavior [3].

In the following the difference between factors, modes and models will be explained.

Factors are environmental variables which contribute to performance loss. The main factors affecting the photovoltaic system are:

- Temperature (static T and cycling ΔT)
- Relative humidity (RH)
- UV rays
- Irradiation
- Mechanical stresses; weight of snow, sand deposits, wind pressure, hail.

Modes are the effect of environmental factors on the module, objective evidence of a failure. The main modes are:

- Corrosion
- Delamination
- Discoloration
- Solder bond weakening
- Hot spots
- Bubbles
- Cell cracking/breaking
- PID (Potential Induced Degradation)
- LID (Light Induced Degradation).

For PV the concept of failure is quite different from any other systems because even if a failure mode is visible the panel could still work and be cost-effective.

But not all modes have the same weight on module performance nor it is simple to understand the evolution chain which brought the undesired effect on the module, in [4] an interesting classification of modes based on technology installation year, climate type and severity ranking is done considering failure rate of older systems and of recent installation, in the last 10 years (since the study was published), and a Pareto chart explain the dominant modes affecting PV, the chart is reported in Figure (2.2-1). Authors collected data of failures intended as degradation modes, defined as 'observable alterations to appearance, performance, and safety of a module', observed their effect on power performance and noted their observation frequency. the risk severity is the aim of FMEA method to analyze efficiently a process aiming to contain risks of failure or defects. The failure mode is how the process could fail, failures are errors or defects, being potential or effective. The effect analysis individuates potential consequences of failure modes, before the item is being marketed and after, during its operational. The severity ranking start at 1, meaning no effect on the module, up to 10, power and safety hazard.

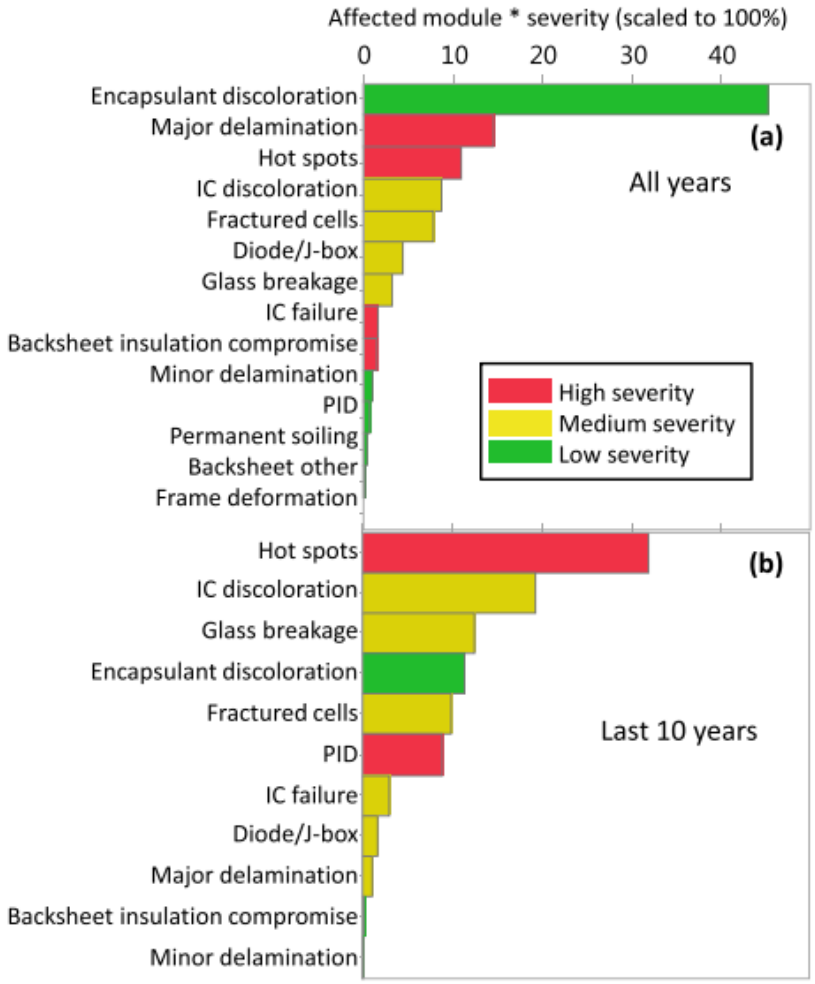

Figure 2.2-1 Pareto chart of the most significant degradation modes [4]

It is possible to notice looking at Figure (2.2-1) the change in prevalent modes during the last 10 years. This is due to technology improvement as the number of impacting modes has decreased, especially encapsulant discoloration, some are decreased but others have become more frequent as Hot Spots; PID on the other hand rank 10 but it is less frequent.

In [5] the main degradation mode was also found with the RPN for c-Si technologies with significant lifespans. RPN is defined in Equation (2.2-1):

$$RPN = S \cdot O \cdot D \tag{2.2-1}$$

Where S, severity, is the single failure mode affecting the performance, O is the probability of occurrence of the failure mode and D is detection. The severity rank is defined with failure rate value (%/year of power loss) of course the higher is the

percentual the higher is the safety and hazardous risk; on a scale from 1 to 10 (10 correspond to high severity). Then the occurrence rank is defined with the frequency of the failure mode recurring in the collected studies; high frequency corresponds to high rank. Detection is not considered.

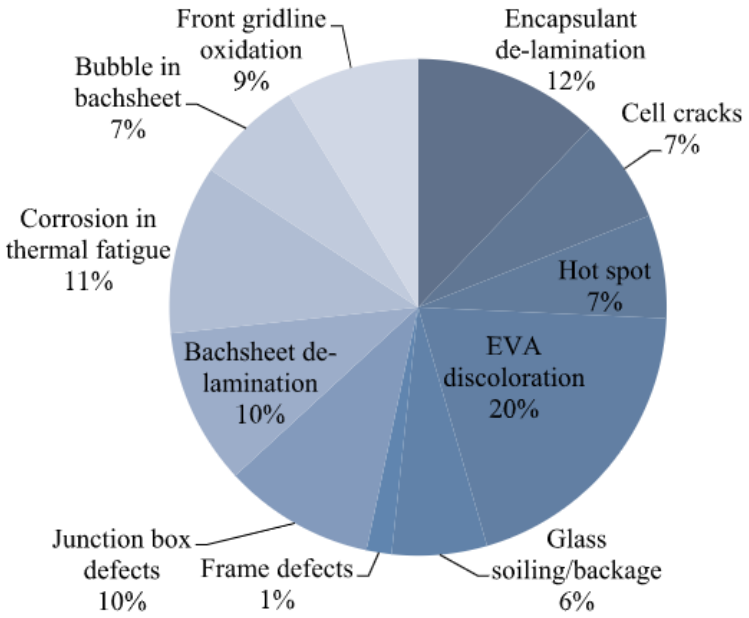

Figure 2.2-2 Percentual Frequency of failure modes occurrence [5]

After ranks assignation for both S and O, RPN is computed. Results are different from [4]; hot spots happen less frequently but are safety hazardous, encapsulant discoloration has PRN 100, very frequent and very dangerous. It could be that results are confused since in this case it was not considered the installation period of the systems considered, the different discrete rank used in [4] and to the failure rates which account more than one mode while severity only refers to a single one. Another aspect to be considered is the number of past studies used to perform the risk analysis.

2.2.1 Corrosion

Corrosion is mainly due to two factors: temperature and relative humidity [10]. Under certain environmental conditions mold can penetrate through the panel sealing, from the back sheet or between two layers, due to bad manufacturing or aging degrade, and deposit between the metallic frame and the protective glass. Corrosion attacks metallic connections and weaken the adhesion between the metallic print and PV cells [10, 11], hence the current collected by the junction box is reduced. Conversely the leakage current increase with more losses and finally the module performance is decreased. It

is a phenomenon which usually start at the edges of the module and with time it spreads toward the center area.

During PV lamination, high temperature process where EVA is melted, acetic acid is released, initially in low quantities later, under an oxidative degradation process, in greater content leading to PV module failure mechanisms, failure modes. Acid corrodes metallic interconnections eliminating the tin used to coats copper core [13]. Furthermore, corrosion of copper leads to brown discoloration of EVA. Generally, corrosion leads to increase in series resistance R_s and performance losses.

Corrosion performance indexes:

- Series resistance R_s [10]
- Normalized power $\frac{P_{\max}}{P_0}$ [12]

2.2.2 Delamination

Delamination happens between encapsulant and back sheet foil and the latter layers, adhesion loss separates cells and encapsulant or encapsulant and the glass back sheet layer [11]. Sometimes gaseous byproduct during manufacturing lamination is trapped inside and their pressure result in layers detachment and bubbles formation [13]. Sometimes, when the surface is bended the probability of other substance ingress increase, this happens for example during the lamination process where pins are used to hold together the module clamp too hard on the surface; moisture can flow in between the layers, starting at the edges till the center of the module area [13]. Delamination effects are metal corrosion and electrical risks. Even a frame not fit for the module can lead to surface deformation. As consequence the amount of light reflected increase and moisture penetrate inside.

Delamination tests are included in IEC 61215.

2.2.3 Discoloration

Discoloration is linked to the dielectric protecting the solar cells, when exposed to intense light the color changes, from the optimal optical transparent, in order to make radiation pass and reach the cells, to yellow or worse brown. The main actors are UV rays. The dominant material is EVA (Ethylene Vinyl Acetate). When oxidation takes place the material releases acetic acid which is entrapped within the module as the whole assembly is fused together. Trapped acid corrodes metallic print reaching the copper core discoloring the EVA as it turns dark brown. Discoloration is unevenly distributed on panel surface, usually at its center. While it does not present a safety issue sometimes can be an indicator of a major problem as when the yellowing is

concentrated around precise spots at high temperature, Hot Spots, or when it presents itself as lines over the cell, in this case it follows the cell crack breaking points [13]. When the encapsulant layer turns darker the light is unable to reach the panel as it was before and as less current is produced as an effect to the series resistance increase, the performance decreases.

Performance index:

- Short circuit current I_{sc} [10, 11]
- $\frac{P_{\max}}{P_0}$ [12]

2.2.4 Light Induced Degradation (LID)

The highest degradation rates happen in the first years of usage of the panel, even if not operated the panel, when exposed to sunlight, degrades up to 1 to 3% in the first hours. To be more accurate this phase is called 'power stabilization' while the actual 'power degradation' happens after [14]. LID is degradation due to sunlight exposure. The amount of power loss is determined by the quality of the silicon wafer used. In fact, it occurs mostly in c-Si and a-SI, where the power reduction can reach 30%, p-type cells [15]. Boron reacts with the oxygen incorporated during the Czochralski manufacturing process. Some authors consider LID as an intrinsic degradation mode which is already take into consideration when power rating is considered [13], others think that although rooted deeply it can be alleviated through an inoculated choice of materials and other particular measures. In p-type Czochralski the degradation due to BO is higher than in n-type mc-Si the value is far less.

Performance index:

- Saturation current used to model the recombination current [15]

2.2.5 Potential Induced Degradation (PID)

As the name implies this degradation phenomena are induced by the high voltage difference between the panel and ground, several hundred of volts, combined with high values of temperature and relative humidity. Modules are connected in series to increase system voltage; high voltages are dangerous so, for safety reason, the metallic structure is grounded. But when insulation wear off, polarization may degrade the electrical panel variables [11]. Even dirt and protective glass can activate this degradation with the release of sodium ions. The performance loss can reach up to 80% of the initial power and severely affect the whole photovoltaic system, luckily in some cases this effect is reversible. The potential difference drives a current flow from the cell to the encapsulant, panel frame and the cover glass leading to power

degradation [3]. The leakage current can be limited if the series resistance R_S is augmented, improvement is carried out choosing different materials for panel glass and encapsulant, making them less conductive and less sensitive to moisture ingress [4]. 'Visible' effect is the black coloration of the cells due to the high potential difference when the panel is inspected with electroluminescence methods [17]. This degradation is so devastating that ad hoc norm was ideated as a pass test for the panel: IEC 62804 [5]. If RH effects are clear and negative, temperature has a duplicity effect as it leads to current decrease but at the same time also to a PID recovery process.

Depending on the technology adopted there are different kind of PID [3, 13, 16]: Potential induced degradation-shunting (PID-s), Potential induced degradation-polarization/passivation (PID-p). While PID-p is reversible and has mild effects, PID-s is rare but extremely dangerous and impacting on panel performance, from the electrical point of view it can be notice a great reduction of shunt resistance, R_{sh}.

The performance indexes:

- R_{sh} [10, 16]
- $\frac{P_{\max}}{P_0}$ [17]

2.2.6 Cell Cracks

Cracks can appear on the module during manufacturing, transportation and installation but can be a consequence of environmental factors: heavy loads like snow or dust, strong winds which may crack the surface leading to disconnection of some cell and high thermal loads can result in a power deficiency with respect to the awaited value [13, 18]. Depending on the gravity of the crack and its conformation on the photovoltaic cell, cell cracks can or not be an actor in power performance. In fact, when a crack is present not all the cell surface is disconnected, but when it is fully disconnected the power loss is proportional to the cell area [18]. As noted in [11] in the years the thickness of cells has gradually decreased while the surface has increased, cells are more fragile than before therefore, cracks probability is higher. A first method to avoid damaged modules to be put in operation is through diagnostic techniques such as optical methods (EL tests, RUV) [18]. The electrical effect of cell cracking is the decrease of I_{SC} since with high temperature resistance tends to increase.

To model cell cracks the following approaches are considered:

- I_{sc} model [10, 15]
- Number of cycles to failure [16]

2.2.7 Hot Spots

Hot spots are small areas of the panel possessing a temperature higher than the module temperature. This effect is caused when the cell is damaged or shaded, the current will be limited and will not flow in the entire string, cells are connected in series. The by-pass diode is used to create an alternative path for the current to flow. In case of problem with the by-pass diode hot spots can be observed with infra-red (IR) inspection especially when the by-pass diode is short circuited, in such case the string will not produce power and the panel overall power production is reduced. When instead the by-pass diode works as an open circuit, as if it were not installed, its effects are hard to detect. Hot spots can be very dangerous, causing overheating and thermal problems to the junction box causing in extreme situation fires.

2.2.8 Bubbles

Bubbles are like Delamination, but they appear only in a limited panel area. Formation is due to trapped gas product of chemical reaction. Bubbles can appear in the back sheet but also on the front side of the panel, in this case high temperature overheats the area and irradiation reaching the surface is reflected [11]. Causes are found in the lamination process.

As conclusion it is necessary to stress that factor combination leads to modes but although studied and explained separately, they can be seen as different steps of the same phenomena. As an example, considering moisture ingress leading to metallic corrosion but as well to loss of adhesion; corrosion and delamination can happen at the same time of at different time instant. So, it is left to the discretion of experts classifying failure modes. The precedent analysis is just a condensed and non-exhaustive summary of what was found in literature.

2.3 Models

To incorporate degradation modes into the reliability study of the module, models are formulated to estimate how they affect the PV module performance. The variety of models found in literature is wide, each of them is based on different approaches: data driven modelling or analytical methods [3, 8]. Data driven can use a statistical approach, machine learning methods or physical based [8]. Data driven approach extrapolate from a set of data (output power of the PV module) the trend to see how the system behaves, this is important as, in time, performance tends to decrease but the causes are to be defined, in fact it could be due to a reversible or irreversible effect,

quantitively the trend is the performance loss in time (%/year). For example, PID and soiling can be reversible (if soiling does not lead to a cementification process) while water infiltration and temperature are irreversible. The analytical approach is more physic/chemic oriented but with a heuristic view [3], in fact it is quite difficult to study all possible material parameters and include them in the model thus the model may not be optimal but just a first approach to the problem.

Many degradation studies observe that the power decrease in time shows two behaviors, in the very first years of operation the panel power loss is great, close to an exponential decrease, and in a second moment the decrease is more stable and follows a linear curve. A PV system enters the fault state when the power decrease with respect to the initial power reach 20% [1, 7, 19].

Studying failure modes is surely a great approach to then implement a model but the model output, power performance, will not depend solely on the studied mode. Most of the time modes happens simultaneously and it is hard to establish which effects correspond to which mode. Models depend on many variables [7]: environmental factors, location, placement characteristic, module technology and design. High amount of data needs to be fed in the model so to accurately formulate and validate it. A good model presents many input factors to realistically follow the power drop over time. But too complex models introduce many parameters making their computation difficult and long.

Modelling degradation could make up for the long observation periods without recurring to AT. But model itself does not refer to a particular degradation mode, they estimate the cumulative loss in power over the years. And considering that models are usually retrieved with AT, as previously mentioned, some modes different from the studied one could manifest [11].

Many authors use just one input factor to simplify the model, recently authors tried to formulate more exhaustive models, multi factors model. And validate them at different locations and climatic zones.

In the following each model found will be briefly explained (based on factor and mode) and its main steps will be record.

2.3.1 Temperature statistical modelling and Arrhenius

In [12] the model proposed combines analytical and statistic approach to model degradation considering temperature as factor. Equation (2.3.1-1) shows the power output degradation:

$$\ln\left(\frac{100}{R}\right) = b \cdot t^{a} \tag{2.3.1-1}$$

R is power percentage with respect to the initial output, a is a parameter associated with material's life, t is time and b is an acceleration parameter which prolong or diminish the module lifetime according to environmental stresses. The external stress is seen through a stochastic process function of time t, $b(s(t))$ with $s(t)$ the instantaneous AF. The time derivative and integral are performed to get the cumulative effect over time. But integrals are difficult to deal so, an average of AF is used instead, $\bar{b}$.

- $b(s(t))$ is the mode, kinetic mode be it chemical or physical
- $s(t)$ is the factor, time series function

Specifically, Arrhenius function models temperature, Equation (A-1) of the Appendix. Equation (2.3.1-2) is obtained rearranging Equation (2.3.1-1) with the above-described steps and converting Equation (A-1) to a log-linear and combining them.

$$\ln\left(\frac{-\ln R(k)}{100}\right) = c_0 + c_1 \cdot \bar{s}(k) + a \cdot \ln(k) \tag{2.3.1-2}$$

Where k is the output power time instant and parameters a, c_0 and c_1 are obtained with OLS method.

Even if authors generally consider the model due to nonspecific modes, in [11] it was classified responding to corrosion and delamination, due to the AT performed, Damp Heat (DH) tests consider combination of temperature and RH which usually trigger corrosion and delamination. This is to be consider a first approach to the problem and not a comprehensive one to study power performance and reliability, degradation depends in fact by contributing factors.

2.3.2 Thermal model

In [15] it is presented a PV equivalent circuit that changes in time considering degradation modes (PID, LID, UV, moisture and cell cracks). The model is time varying and nonlinear. The performance index is the normalized efficiency.

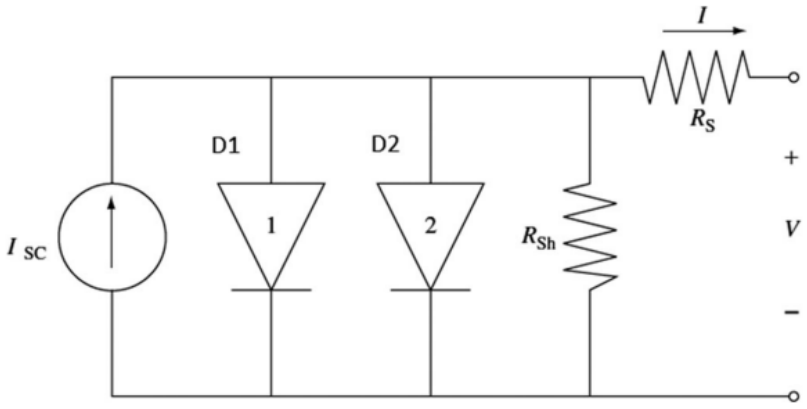

Figure 2.3-1 Equivalent PV circuit [15]

Degradation is modelled with element variation.

- PID → leakage current (glass, top cell, EVA, back sheet)→ R_{sh}, Equation (2.3.2-1)
- LID → recombination current in the base → saturation currents I_{01}, I_{02} in the diodes, Equation (2.3.2-2)
- UV Discoloration → DYI, Equation (2.3.2-4) → R_s and R_{sh}, Equation (2.3.2-5, 2.3.2-6)
- Moisture → R_s , Equation (2.3.2-7)
- Cell cracks →photo generated current and the recombination currents, Equation (2.3.2-3)

The model proposed is a thermal model. Temperature is the main factor; the thermal model considers heat fluxes:

- external heat fluxes (irradiation taken as sine function)
- internal heat fluxes (joule effect of R_s and R_{sh})
- operating conditions (V)
- heat dissipation (convection and radiation)

The PV module is built into a simulator with input of G, T, wind speed and V; then it tested in a laboratory experiment and the in situ, the factors are averaged. Then model inputs were derived and fed into the derived Equations (2.3.2-1 to 2.3.2-7) their outputs are included into the PV cell model and finally Normalized efficiency (NE) and power output are plotted, Figure (2.3.4-2).

$$R_{sh1,deg} = \frac{1}{\alpha_1 \cdot V_{op}^2 \cdot RH^2 \cdot \exp\left(\frac{-E_a}{R \cdot T_{avg}}\right) \cdot t^2} \qquad (2.3.2\text{-}1)$$

Where V_{op} is the operational voltage, RH relative humidity, R gas constant 8.314 (J/mol K), E_a activation energy, T average temperature and t time.

$$I_{01,deg} = I_{01,T_{1,STC}} \cdot \alpha_2 \cdot \frac{G}{1000} \cdot exp\left(\frac{-E_a}{R \cdot T}\right) \cdot t$$
$$I_{02,deg} = I_{02,T_{1,STC}} \cdot \alpha_2 \cdot \frac{G}{1000} \cdot exp\left(\frac{-E_a}{R \cdot T}\right) \cdot t \quad (2.3.2\text{-}2)$$

Where G is irradiation and T temperature.

$$\begin{cases} I_{SC,deg} = I_{SC,T_{1,STC}}\left(1 - \frac{A_{inactive}}{A_{total}}\right) \\ I_{01,deg} = I_{01,T_{1,STC}}\left(1 - \frac{A_{inactive}}{A_{total}}\right) \\ I_{02,deg} = I_{02,T_{1,STC}}\left(1 - \frac{A_{inactive}}{A_{total}}\right) \end{cases} \quad (2.3.2\text{-}3)$$

$A_{inactive}$ inactive cell surface and A_{total} total cell surface.

$$DYI = \alpha_3 \cdot \exp\left(\frac{-E_a}{R \cdot T_{avg}}\right) \cdot G_{avg} \cdot \log\left(\frac{t}{3600}\right) \quad (2.3.2\text{-}4)$$

DYI delta yellowing index and G_{avg} average irradiation.

$$R_{s,deg} = R_{s,T_{1,STC}} + \alpha_4 \cdot DYI \quad (2.3.2\text{-}5)$$

$$R_{sh2,deg} = R_{sh,T_{1,STC}} - \alpha_5 \cdot DYI \quad (2.3.2\text{-}6)$$

$$R_s = \alpha_6 + \alpha_7 \exp\left(-\frac{E_{a_1}}{R \cdot T}\right) \cdot \sin(Dist) \cdot \exp\left(-\frac{E_{a_2}}{R \cdot T_{avg}}\right) \cdot RH \cdot t \quad (2.3.2\text{-}7)$$

$Dist$ is the normalized distance from the center

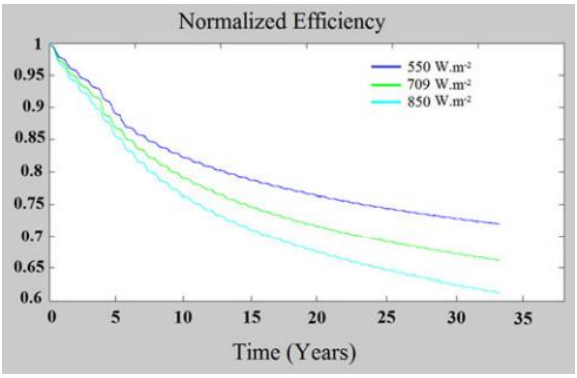

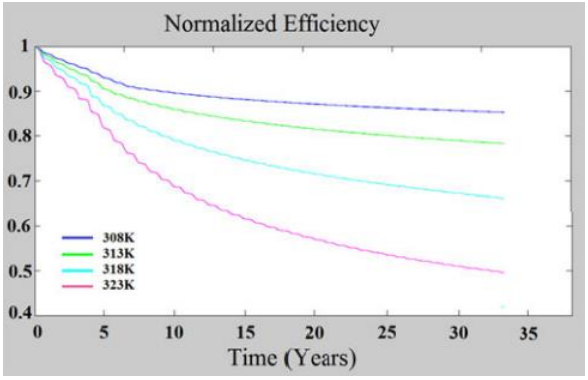

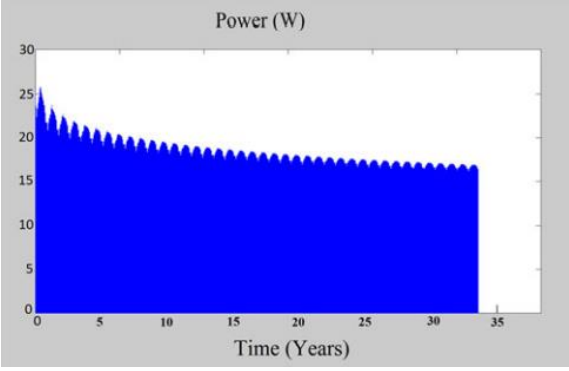

Figure 2.3-2 model results, NE(G), NE(T) and P in years [15]

The model considers degradation, thermal behavior and operating conditions. The aim was to prove that degradation process is not uniform. The model is applied to mc-Si and is constrained by validity ranges, 200-1200 W/m² and 233-353 K, wind speed range is 0-10 m/s. Results show nonlinear behavior of degradation and a quick loss in efficiency during the first operational years. During summer high T leads to a prominent decrease of NE while in winter the rate is lower, this explains the wavelet shape of Figure (2.3.4-2). Validation comes from comparing degradation trends of other studied with this model results confirming a high drop in power in the first years which later diminish.

2.3.3 Solder joints model

A model on solder damage is studied in [20]. The model is based on damage accumulation over time and dependent from weather inputs. The Coffin-Manson and Norris-Landzberg equations are used, Appendix Equation (A-2, A-3). In Equation (2.3.4-1) is the solder damage.

$$D = C \cdot (\Delta T)^n \cdot \left(r(T)\right)^b \cdot \exp\left(-\frac{E_a}{k_B \cdot T_{\max}}\right) \qquad (2.3.4\text{-}1)$$

D is the accumulated damage, C is a constant, ΔT is the mean daily maximum temperature, $T_{\max}$ is the mean daily maximum temperature, E_a is the activation energy, k_B is the Boltzmann constant and finally $r(T)$ is the reversal term, the number of time temperature increases or decreases during the year across temperature T. The equation is fitted to the acquired data of simulation, via a FEM model. In Figure (2.3.4-1) is presented the comparison of simulation results and model results with different frequency measurement resolutions.

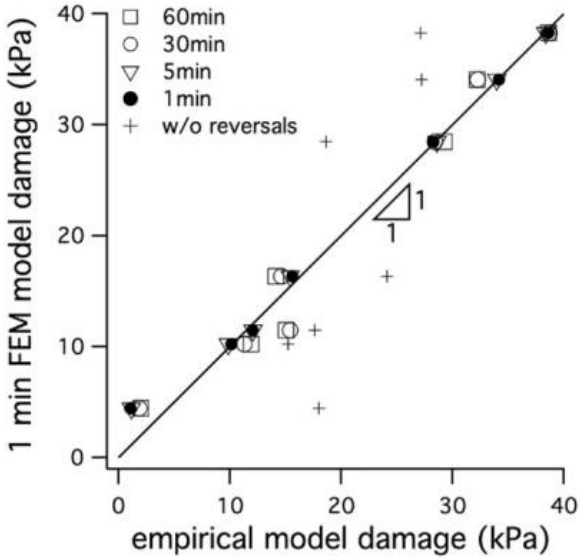

Figure 2.3-3 FEM simulation vs model results [20]

The cross symbols in Figure (2.3.3-1) refers to results without reversal term, it can be noted that they are far from the unity line.

Assumption and simplifications were made such as considering only the bottom layer solder damage, the temperature was modelled instead of using the module', for generalization's sake. Only temperature is considered as factor.

2.3.4 PID models

- In [16] PID is studied so to estimate actual stress during the module lifetime in a specific location. The model only considers PID as mode, product of T and RH factors, through R_{sh} evolution under variation of the I-V slope at V=0. Both shunting and regenerative behavior are contemplated even if the aim of the thesis is to deal with irreversible effect on the module due to degradation. A strong point is the validation process with real outdoor data recreating similar conditions to the laboratory. Ambient data were translated to module data (NOCT for temperature and Magnus formula for RH, Appendix Equation (A-4, A-5). The R_{sh} evolution is observed in Figure (2.3.4-1).

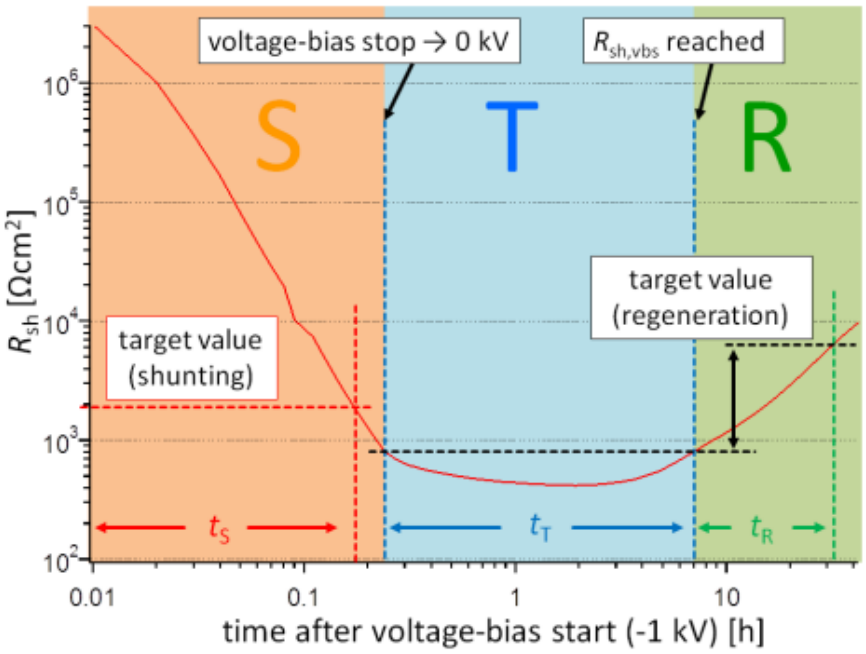

Figure 2.3-4 R_{sh} time evolution at constant temperature with phases: shunting, transition and regeneration [16]

The time intervals are determined with the phase assignment criteria illustrated in Figure (2.3.4-2). Where IR_{mod} is module irradiation. The conditions for T-phase are expressed in Figure (2.3.4-1), extremes of dashed lines.

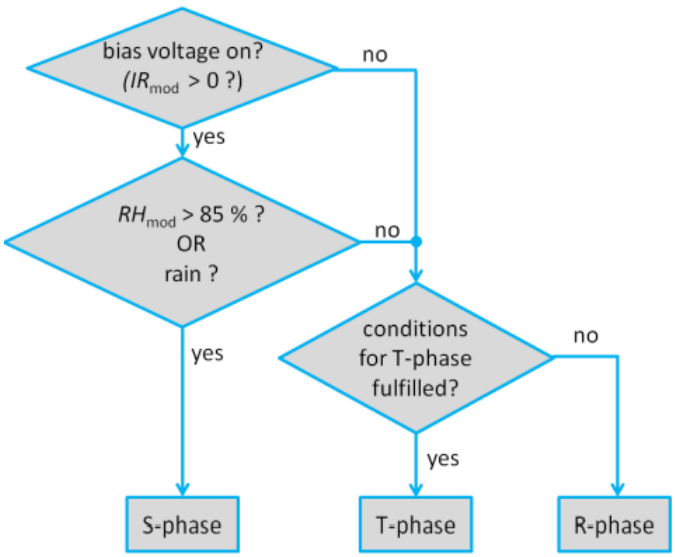

Figure 2.3-5 phases assignment criteria [16]

Time dependent empirical formula describe the shunt resistance evolution, values combination of T_{mod} and RH_{mod} assign the R_{sh} phases and give the time steps amplitude: t_S , t_T and t_R .

$$R_{sh}(t) = a_s \cdot \exp\left(-\frac{t}{b_s(T_{\mathrm{mod}})}\right) \tag{2.3.4-1}$$

$$R_{sh}(t) = c_R + a_R \cdot \exp\left(\frac{t}{b_R(T_{\mathrm{mod}})}\right) \tag{2.3.4-2}$$

$$R_{\mathrm{sh}}(t) = a_T(T_{\mathrm{mod}}) \cdot \left(t + b_T(T_{\mathrm{mod}})\right)^2 + c_T \tag{2.3.4-3}$$

The constants a_s, a_R,, a_T,(T_{mod}), b_S,(T_{mod}), $b_R(T_{mod})$, b_T (T_{mod}), c_R, and c_T are specific to the module type and are determined using the time intervals of each phase, t is time, T_{mod} is module temperature. Equation (2.3.4-1, 2.3.4-2) are Arrhenius like while Equation (2.3.4-3) is a polynomial.

Models and data show little discrepancies, the model is assumed to be accurate though uses quite simple formulas. Nevertheless, authors stress on the data frequency acquisition which may overestimate end results in case of rain or dew, weather data overestimation particularly for rain events, further decrease in the shunting phase can lead again to overestimation. Results only show a confront on R_{sh} not on power.

- In [17] formulate a PID model based on Peck formula, Appendix Equation (A-6) and exponential model dependent on temperature and relative humidity. The data used is semicontinuous and statistical power degradation and leakage current, obtained by in-situ dark I-V measures in an environmental chamber. Accelerated tests with different combination of T and RH (60°C/85%, 72°C/85%, 85°C/85%, 60°C/95%, 60°C/100%) are performed on PID resistant modules (pc-Si), then the dark I-V curve is obtained along with Pmax and normalized Pmax with reference at maximum power at STC. The TTF with Peck and exponential behavior are reported in Equation (2.3.4-4) and Equation (2.3.4-5) respectively.

$$TTF = A_0 \cdot f(V) \cdot \exp\left(\frac{E_a}{k_B \cdot T}\right) \cdot RH\%^{-B} \quad (2.3.4\text{-}4)$$

$$TTF = A_0 \cdot f(V) \cdot \exp\left(\frac{E_a}{k_B \cdot T}\right) \cdot \exp(-RH\% \cdot B) \quad (2.3.4\text{-}5)$$

E_a is the thermal activation energy, A_0 the pre-exponential constant, B is the exponential of RH, RH the relative humidity (%), k_B the Boltzmann constant, T the temperature and $f(V)$ is a function of the voltage which is considered constant. The reciprocal of Equation (2.3.4-4) is the degradation rate, the term after the subtraction operator in Equation (2.3.4-6), which shows the Peck model.

$$\frac{P_{max}}{P_{\max\_0}} = 1 - A \cdot \exp\left(-\frac{E_a}{k_B \cdot T}\right) \cdot RH\%^{B} \cdot t^2 \quad (2.3.4\text{-}6)$$

At the left side there's the power, at the right the degradation model function of time t.

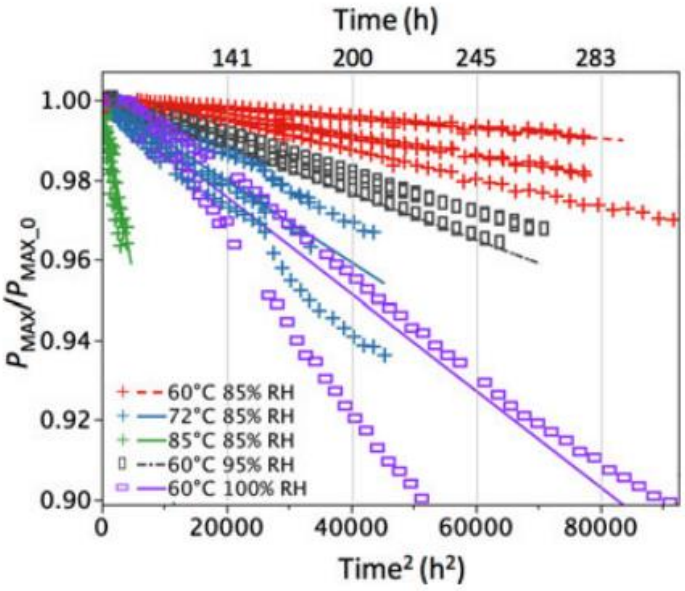

Figure 2.3-6 Data and model prediction on a time-squared axis [17]

Parameters are extracted applying the OLS method on the data set. Linearization is useful only if the degradation is known to follow it. The AT

duration reaches 700 h but the linearized power is fitted only for 300 h (90000 h^2) meaning that only initial PID effect is modelled due to the linear range.

Results show that humidity plays a bigger role in PID, with the accelerated model performance of the module is retrieved with quicker experiments but only when the model behaves linearly.

2.3.5 Physical Multi stressor model

In [7] is studied a multi precursors (hydrolysis-T, RH photo-degradation-UV, RH, T thermo-mechanical degradation-ΔT, T_{max}) model with P_{mpp} as the performance index, Equation (2.3.5-1).

$$\frac{P_{MPP}(t)}{P_{MPP}(0)} = 1 - exp\left(-\left(\frac{B}{k_i \cdot t}\right)^{\mu}\right) \tag{2.3.5-1}$$

$P_{mpp}(t)$ is model output at time t, B is the power susceptibility, property of the material, μ is the shape parameter; these parameters depend on the module materials, technology and design, while B changes as technology improve or not, μ, the shape parameter, adjust the model curve to data. This formulation is implemented to avoid using too many, specific to the module, parameters. k_i is the degradation rate constant of process i. The three kinetic models corresponding to each degradation precursor are given in Equation (2.3.5-2 – 2.3.5-4).

$$k_H = A_H \cdot rh_{eff}^n - exp\left(-\frac{E_H}{k_B T_m}\right) \tag{2.3.5-2}$$

$$k_P = A_P \cdot (UV_{dose})^X \cdot \left(1 + rh_{eff}^n\right) \cdot \exp\left(-\frac{E_P}{k_B \cdot T_m}\right) \tag{2.3.5-3}$$

$$k_{T_m} = A_{T_m} \cdot (\Delta T)^{\theta} \cdot C_n \cdot \exp\left(-\frac{E_{T_m}}{k_B \cdot T_U}\right) \tag{2.3.5-4}$$

A_H, A_P, A_{T_m} are gain constants, E_H, E_P, E_{T_m} are activation energies for each degradation precursor, rh_{eff}^n is RH, T_m is the module temperature, T_U is the upper temperature, UV_{dose} is the UV amount, ΔT is the thermal difference, C_n is the cycling rate, k_B is the Boltzmann constant and n, X, θ are parameters to be determine.
The degradation rates are assumed working both independently and dependently, the total degradation rate is given in Equation (2.3.5-5).

$$k_T = A_N \cdot \prod_{i=1}^{n}(1 + k_i) - 1 \qquad (2.3.5\text{-}5)$$

The model is tested for three different climatic conditions; maritime, arid and alpine, weather inputs are average to confirm lab results are in line with outdoor data. The modules are from the same manufacturer and are made with mc-Si. Weather measurements are gathered for five years. The model is validated with indoor and outdoor data. In case of outdoor validation only clear sky condition is considered, degradation due to soiling is not contemplated as the modules were periodically cleaned. The model is calibrated on the data set through a data fit.

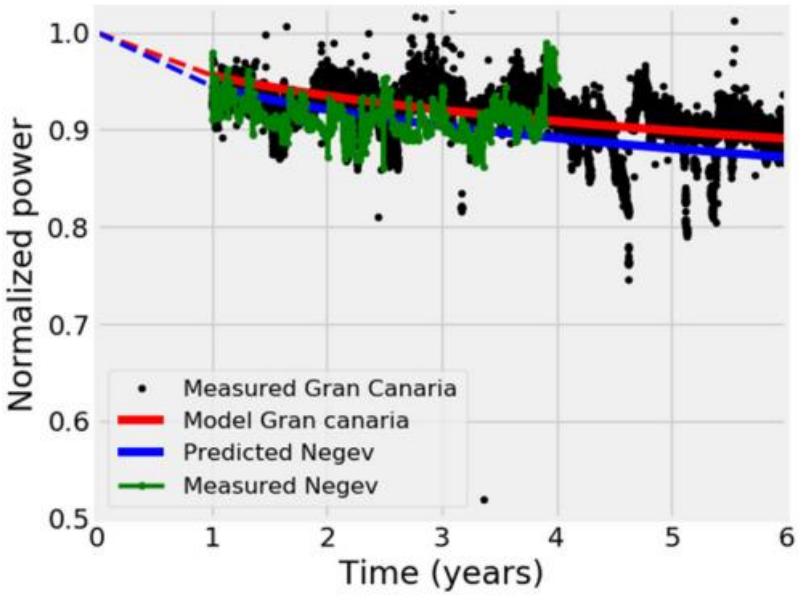

Figure 2.3-7 model prediction vs measurements [7]

The model is T dependent as Arrhenius formula is present in all kinetics. Moreover, assumptions are made on the dominating mode happening, averages values of weather conditions are taken instead of using stochastic approaches and AT are taken with caution trying to implement non extreme test conditions which could lead to high uncertainties and mode misinterpretations and bad correlation with outdoor conditions.

2.3.6 Cumulative model

Another model which considers multiple modes is formulated in [19]; it considers the cumulative effect of weather inputs. It considers the model degrade y, as the actual degrade G plus an error ε. The actual degrade is computed as a sum (integral in time of weather stresses s) yet it is considered the dynamic of inputs rather than averages, Equation (2.3.6-1).

$$y(t_{ij}) = G[t_{ij}, x_i(t_{ij})] + \varepsilon_i(t_{ij}) \tag{2.3.6-1}$$

$$G[t_{ij}, x_i(t_i)] = \beta_{in} + \int_0^t \prod_{l=1}^{p} f_l[x_{il}(s), \beta_l]\, ds \tag{2.3.6-2}$$

$$y_i(t_{ij}) = \beta_{in} + \sum \beta_0 \cdot \prod_{l=1}^{p} f_l[x_{il}(t_{il}), \beta_l] + \varepsilon_{ijl} \tag{2.3.6-3}$$

Where i denotes the modules, j is the number of points when degradation measures were taken on module i. t is time, β_{in} initial level of power degradation (-0.1 considering intrinsic uncertainties), the degrade is function of the instantaneous effect of stresses $x(s)$, p is the number of factors/modes considered.

Equation (2.3.6-3) is the final form of the model; the form is discrete as data on weather is discrete. The term $f(\cdot)$ is explicated with rate equations (Arrhenius for T, Coffin-Manson for ΔT and Peck for RH) while UV is 5% of plane of array irradiance, Equation (2.3.6-4).

$$\begin{aligned} R_D(T, \Delta T, UV, RH) &= \beta_0 \cdot exp\left(-\frac{\beta_1}{k \cdot T_{max}}\right) \cdot \left(\Delta T_{daily}\right)^{\beta_2} \cdot \left(UV_{daily}\right)^{\beta_3} \\ &\cdot \left(RH_{daily}\right)^{\beta_4} \end{aligned} \tag{2.3.6-4}$$

β_0 is the frequency factor, β_1 is the activation energy, β_2 -β_4 are the effect of term in the corresponding brackets.

The rate equation is included in the cumulative damage model. And parameters are estimated with a genetic algorithm given the nonlinearities and bounds of parameters. In Figure (2.3.6-1) final results are shown, with satisfactory values. The out of bounds values are of unknown origin so they cannot be omitted.

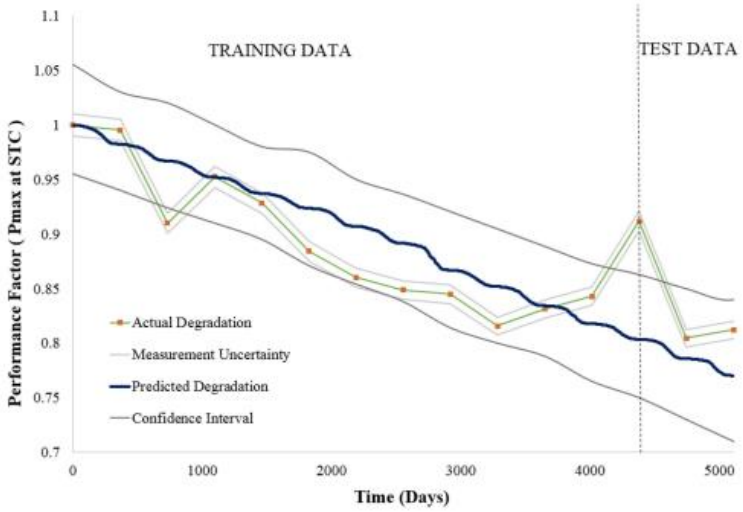

Figure 2.3-8 Actual degradation vs predicted, training and validation data [19]

In this model only some modes are considered while other, of equal importance are left out, moreover it was used ambient RH instead of module'. The model is applied only to mc-Si technologies. The model is an upgrade version of [12] and needs high amount of data to be implemented with relative costs.

2.3.7 Circuit parameter models

In [10] a model dependent on temperature, relative humidity, UV radiation, voltage potential between module and ground and thermal cycles is studied. Every degradation mode has its own model. Simulations are performed considering three different climate zone (Mediterranean, hot and dry and hot and humid). It is based on the double diode model which works better at low irradiance levels, Figure (2.3.2-1). Empirical laws are found looking at the evolution of the model parameters during ATs.

- Corrosion $\rightarrow R_s$
- Discoloration $\rightarrow I_{sc}$
- PID $\rightarrow R_{sh}$
- Cell cracks $\rightarrow crack\ activation_t$

Corrosion follows the Peck model, Appendix Equation (A-6), rate of degrade which is incorporated into R_s Equation (2.3.7-1) obtained from ATs.

$$R_S = R_{S_0} + \exp(R_D \cdot t - B) \tag{2.3.7-1}$$

R_{S_0} is the initial series resistance, t is time, R_D rate of Peck formula and B is a constant. UV cumulated is 5.5% of the light spectrum. EVA discoloring has a linear degradation of 10% at the end of module' lifetime. AT performed showed a decreasing exponential trend.

$$I_{sc}(t) = I_{sc_0} - a \cdot D_{UV}(t) - b \cdot \left(1 - \exp\left(-c \cdot D_{UV}(t)\right)\right) \tag{2.3.7-2}$$

I_{sc_0} is the initial value of short circuit current, $D_{UV}(t)$ the UV dose (MJ/m²) about 5.5% of the light spectrum $E(u)$, Equation (2.3.7-3), a,b and c are coefficients.

$$D_{UV}(t) = \int_0^t E(u) \cdot 5{,}5\%\, du \tag{2.3.7-3}$$

PID is linked to leakage current, used as degradation rate, Equation (2.3.7-4).

$$R_D = A \cdot V \cdot \frac{B}{1 + \exp(-C \cdot RH + D)} \cdot \exp\left(-\frac{E_a}{k_B \cdot T}\right) \tag{2.3.7-4}$$

V is the voltage applied, RH is the relative humidity, E_a the activation energy, k_B the Boltzmann constant, T the module constant, A, B, C and D are parameters. R_{sh} is modelled in Equation (2.3.7-5).

$$R_{\mathrm{sh}} = \frac{R_{sh_0}}{1 + a \cdot R_D \cdot t} \tag{2.3.7-5}$$

R_{sh_0} the initial value of shunt resistance, R_D the degradation rate, t is time and a is a parameter. All listed parameters have been obtained with data fit to the ATs data. Activation energies are retrieved from other studies.

Cell crack depends on thermal variation which act on I_{sc}, the probability of a cracked cell is of 5%, then the inactive cell surface will increase from 0 to a certain amount linearly. The amount is determined by a gaussian distribution with mean 8% of the cell surface and standard deviation of 2%. I_{sc} is then multiplied by the active cell surface $(1 - S_{inactive}(\%))$.The crack activation is modelled in Equation (2.3.7-6).

$$Crack\ activation_t = Crack\ activation_{t-1} + \frac{1}{x \cdot \left(\frac{125}{CT}\right)^m} \quad (2.3.7\text{-}6)$$

x is the thermal cycle, CT is the daily temperature amplitude and m is a parameter.

The power from AT is expressed in Equation (2.3.7-7).

$$p_{indoor}(t,T) = \frac{1+\exp(-B)}{1+\exp(R_D(T,RH)\cdot t - B)} \quad (2.3.7\text{-}7)$$

The next step is to find a link between indoor test results and outdoor, the extent of reaction is the advancement state of the phenomenon, from 0 to 1, useful to iteratively estimate power evolution outdoor, X, a decrease of relative power from one. Now the time necessary to reach the same extent also in indoor condition with constant temperature is the equivalent time, reciprocal of the indoor power. Deriving the power formula considering the equivalent time and temperature the power slope is obtained which is integrated in Equation (2.3.7-8).

$$p_{outdoor}(t) = \int_0^t \dot{p}\left(t_{eq}(T,X),T\right) du \quad (2.3.7\text{-}8)$$

Results are showed in Figure (2.3.7-1).

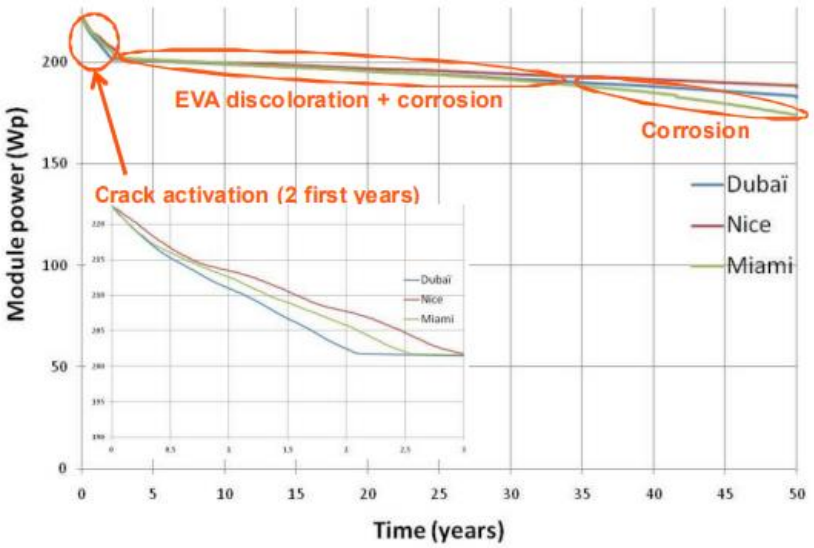

Figure 2.3-9 model results for 50 years at different locations [10]

2.4 Degradation Rates and Preventive Actions

Along with the warranty period, manufacturers indicate the degradation rate of the panel, a percentual per year of constant power loss. The lower its value the better the module performs. Degradation rates are based on the simplified assumption that degrade is linear which is not entirely wrong but not accurate either. Degrade in PV modules follows the bath tub plot, Figure (2.4-1), a fast degrade during the infant phase, a stable behavior for most of its lifetime and a quick wear out phase at the end. As shown in the output of models in the previous paragraph, the degrade is nonlinear and follows a seemly decreasing exponential trend. Many authors tend to not consider the initial part since it is usually linked to LID stabilization, others consider it as already happened thus just consider the linear degrade part. Long term yield depends on performance and efficiency. LID can cause an efficiency loss of 15% in the first years. Considering degrade on I-V curve parameters (maximum power P_{max}, short circuit current I_{sc}, open circuit voltage V_{oc} and fill factor FF) in most of studies analyzed the decreases in power is sensible to short circuit current reduction while open circuit voltage and fill factor remain almost stable, this is not always the case since electrical parameters depend by the cells' technology employed. Cell cracks are dormient and later activate with certain temperature condition. Encapsulant discoloration decreases power gradually in time. As previously mentioned, it is easy to see the power drop but it is quite difficult to establish which failure mode or which aesthetics defects cause it.

Relating degradation rates to a certain failure mode can be useful in order to predict when to perform maintenance on the model-based algorithm which will be presented later in this study. Algorithm maintenance shall be performed every time there is a substantial power loss not attributable to a reversible event affecting the module. To set thing right ordinary maintenance and periodical cleaning shall be assumed.

As module degrade, each electrical parameter drift from the reference value indicated in the product' datasheet. The most important to check out is the reference power.

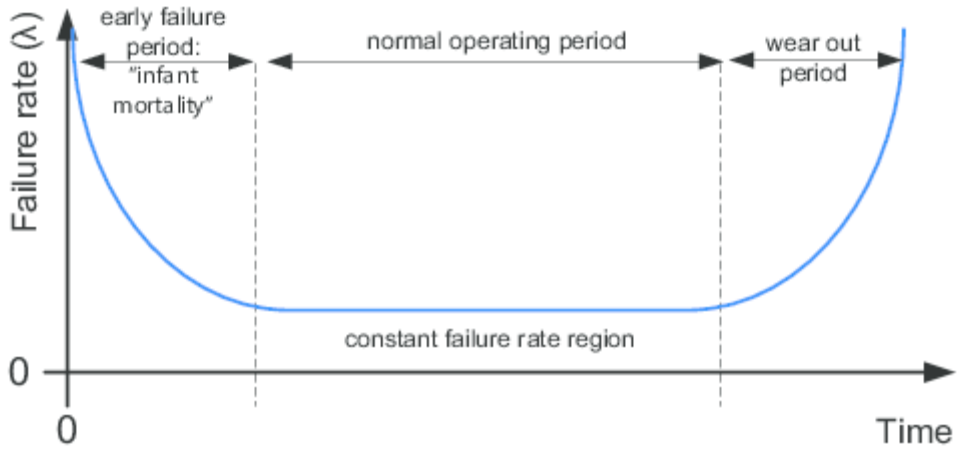

Figure 2.4-1 Bath tube graph

Reconsidering the previous paragraph, in Figure (2.3.7-1) the final plot of power prediction shows an initial decline due to cell cracks in 2 to 3 years with a rate of -0.036% over the said period, then a slightly decrease due to discoloration and corrosion (up to 25 years) and then a higher reduction due to corrosion. Lab test percentage reduction are around or less than 20%, in line with the manufacturer set warranties.

In Figure (2.4-2) is reported an accumulation of data indicating the main failure modes happening throughout all operational years of the PV system with their frequency, with the below picture showing failures which bring a substantial power loss [25]. Maintenance and cleaning are key to maintain high system performance. First to notice is that most power losses are due to soiling which is reversible if a periodical cleaning is performed. Then the failures in the first years are linked to cell cracks (1-2 year), PID (3-4 year), disconnected cells (after 4 years and constant declining over the lifetime), discoloring after 3 years and so on. By pass diode defects are spread over the first 10 years. Causes of power losses are environmental loads such as hail, snow, storms effect, direct lightning and animal traces; the paper specifies how much power is lost due to each failure mentioned, Figure (2.4-2) with Table (2.4-1) for a better understanding, relative to moderate climate.

Delamination	7%/y
Back sheet	-
Junction box	10%/y
Discoloring	0.2%/y
Cell cracks	5%/y
Hot spots	6%/y
PIDs	18%/y
PIDc	14%/y
Cells disconnection	21%/y
By pass diode	25%/y
Corrosion	-
Glass breakage	3.5%/y
Back sheet	3%/y

Table 2.4-1 degradation rates (approx.) related to Figure (2.4-2)

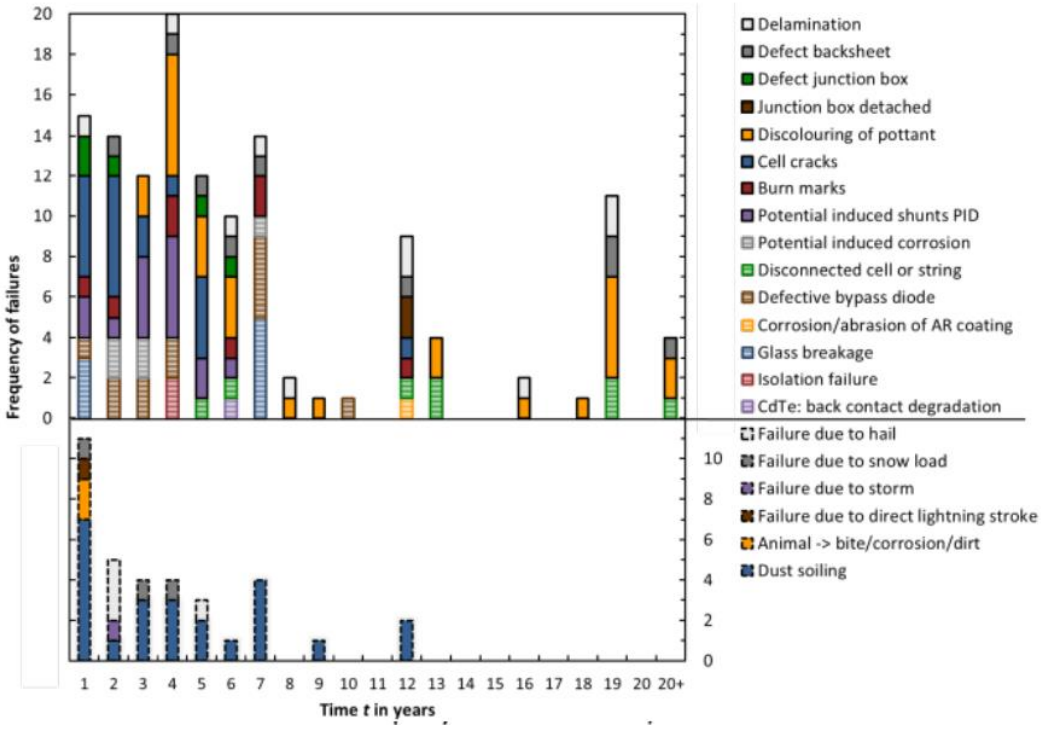

(a) failure mode frequency throughout module' life

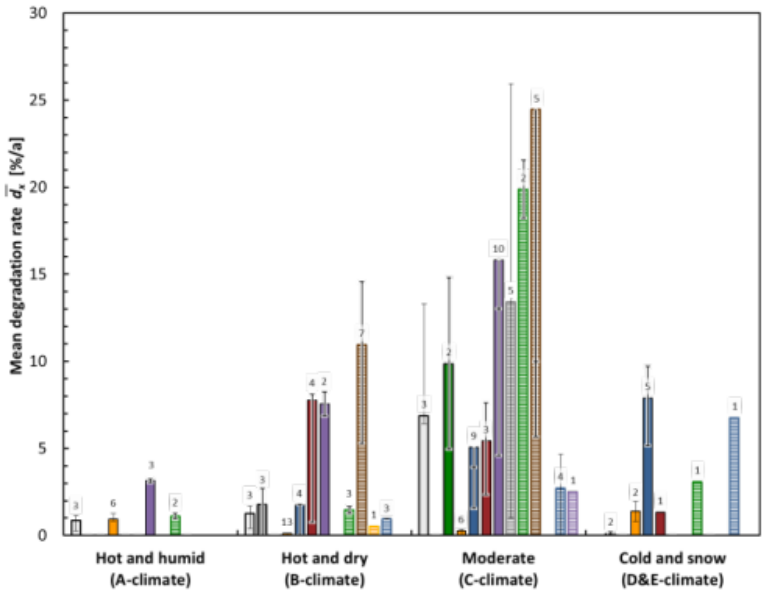

(b) degradation rates related to modes for different climate

Figure 2.4-2 failure mode distribution throughout module lifespan and relative rates [25]

In Figure (2.4-3), [21], another observed PV power behavior is reported. LID is not considered at all (the module is pre exposed to light effects) as it affects all modules. Most common and not dangerous failure mechanisms are present during all module' lifetime such as discoloration, delamination, losses due to AR coating and cracked cells. The figure shows also more than one possible scenario linked to the phases of the bath tub graph.

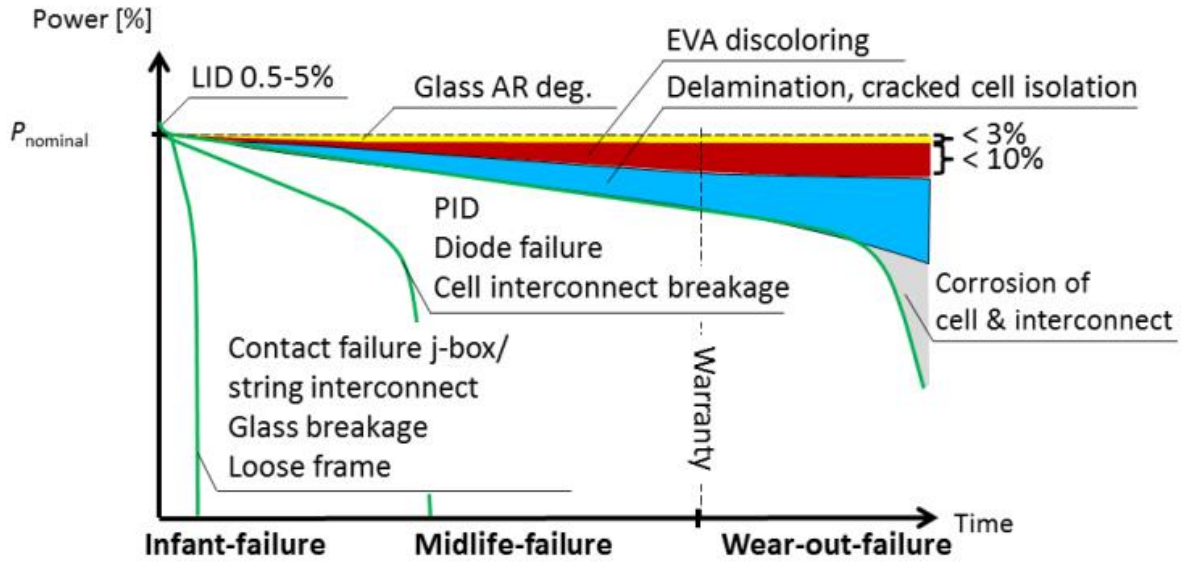

Figure 2.4-3 summary of failure scenarios during PV lifetime [21]

Some studies also indicate degradation rates linked to failure modes and I-V curve parameters: P_{max}, I_{sc}, V_{oc} and FF as in [22, 23, 24].

	Pmax	Isc	Voc	FF
EVA discoloration	12.5-26.4%/10 y (1.25-2.64%/y) 0.85-1.1%/y	8-19.4%/10 y (0.8-1.94%/y) main factor		
Cell discoloration	2.16–2.76%/ y	1.08–1.2%/year	0.16–0.32%/y	1.05–1.52%/y
EVA delamination	1.97-3%/y overall 1.8-2.85%/y linear	Main factor		

Snail trails	1.6–3.42%/y linear 1.81–3.56%/y overall	0.9–1.68%/y		0.98–2.15%/y
Soiling	6.4% to 11.3%/10 y			
Cell cracks	2.4%/y linear average 6%/y			Main factor
Glass breakage			0.72–1.13%/y main factor	
Hot spot	4.5-5.5%/y 1.29%/y (1 module with hot-spot) 1.63%/y (5 modules with hot spot)			Main factor
PID	4.5-7%/y			Main factor
Back sheet	4.22%/y overall 4.09%/y linear			
LID	4.5-6%/y 3%/y			Main factor
By pass diode	1.58%/y			

Table 2.4-2 collection of degradation rates affecting I-V curve parameters

.

3. Power Control

In this chapter the issue of frequency regulation will be studied from the point of view of photovoltaic. After an introduction on the traditional way of handling the problem, it will be explained how a static converter, such as PV, can contribute and what are the recent strategies studied.

3.1 Introduction

PV systems can be connected to the grid in industrial and residential applications or exist as a stand-alone system. The first approach is the most diffused, whether it is a solar plant or just a couple of PV panels mounted on the roof of a private residence [3]. This is due to the nature of the primary energy, sunlight. In fact, light is available only during daytime and if weather conditions permit it. Because of its intermittent nature, the lack of energy must be supplied by something else, the electrical grid. At the same time photovoltaic low efficiency leads to operate them at their maximum power point without possibility of control over their output [1, 3]. Grid connection brings many advantages; economic such as the possible revenues if the solar power exceeds load consumption, most of the time storage batteries are not installed hence battery losses are null and the project cost is lower. On the other hand, always in case overproduction of power, the difference between produced power and power consumed by the photovoltaic systems is injected into the distribution grid leading to issues in frequency regulation. A permeated system with RES solutions like PV can pose a problem to the grid stability and reliability. Usually, traditional system generators like rotating machines, thanks to their masses, contribute to the grid stability regulating its frequency using their inertia but in a system with high penetration of RES, inertia response significantly decreases [2]. A recent issue regarding solar panels is their use to regulate grid frequency. But how can a static component as it is a PV panel contribute to this problem? The solution resides in the control of the power output of the solar system.

3.2 Traditional Frequency Regulation

A power system is characterized by two parameters: voltage and frequency. To supply all loads without unwanted interruption voltage and frequency must fall into predefined limits. Frequency regulation is employed every time the grid frequency grid deviates from 50 Hz (or 60 Hz depending on the country) with some acceptable tolerance degree, 49,0 Hz-51,0 Hz; when the range widen the electrical system enters emergency state and generators are allowed to work for a short time under these conditions. If a small deviation can be adjusted with relative ease, acting on the generators involved, a large deviation will lead to a great grid instability. The cause in this phenomenon is the power balance, when generation does not match load demand and vice versa [3]. If power generation is more than the load demand the grid frequency will rise (over-frequency), else the grid frequency will drop (under-frequency).

Over-frequency events are easily managed as increase in grid frequency is slow so the system operator can reduce the power generated. Under-frequency events are often unexpected and cause large loss of electricity; to reverse this effect three controls are triggered:

- primary frequency control (inertial response and governor response); it is automatic, generators involved in PFC will adjust their output in few seconds, it consists of inertial response, synchronous generators kinetic energy exchanged to readjust frequency value, and governor response
- secondary frequency control, also called AGC (Automatic Generation Control), happens right after the primary, it takes more time, and its purpose is to restore the nominal value of frequency with designated generator for this task
- tertiary frequency control (reserve deployment); the system needs to restore the reserve margin used for frequency regulation, it is the only manual control, and it is executed on express request of the grid operator

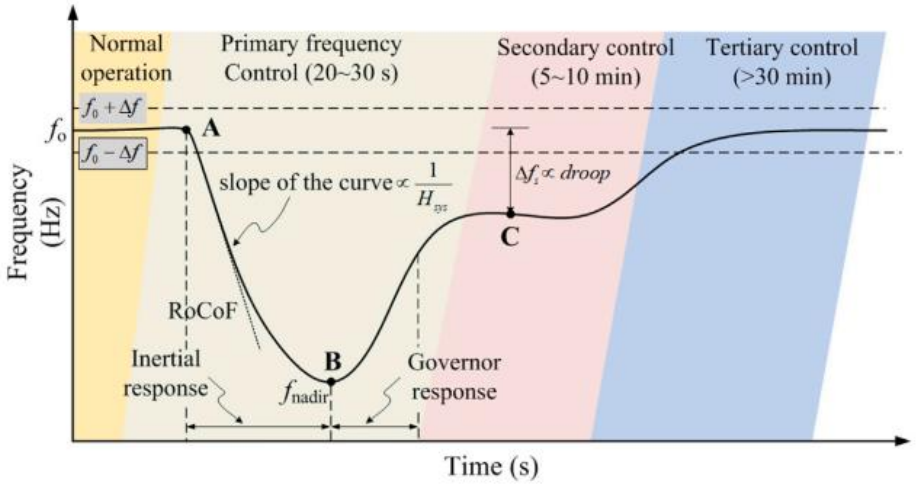

Figure 3.2-1 Frequency response, the control stages are highlighted [3]

3.3 PV contribution

PV installations lead to reducing operation of other plants which may contribute actively to the frequency regulation and, since photovoltaic systems are not schedulable, this poses a problem to the electrical network stability, operability and service interruption. Another problem is the surplus power injected into the grid which may also cause power unbalances.

PV systems can contribute to frequency regulation:

- Power curtailment
- Energy storage system (ESS), keeping the PVs in the MPPT mode, the energy stored in batteries can be used when needed
- Power control strategies. This is possible with a control logic.

Curtailment is a progressive power reduction with final disconnection from the grid, it leads to unsupplied loads which could undermine service continuity, not desired as the service cannot be interrupted arbitrarily. ESS, specifically BESS, can store inside PV power and act on frequency deviations with an amount of power higher than the MPP and even in low power production periods like during nighttime. Yet batteries are expensive; considering actual cost, maintenance and possess limited lifetime [5].

3.3.1 Power Control Strategies-Review

Recently, PV systems can provide ancillary services adjusting the active power produced to regulate frequency. In this review will consider solutions with PV participation without rely on BESSs:

- CPG
- DPC
- Modified fractional V_{oc}
- P-f droop characteristic
- Multi control

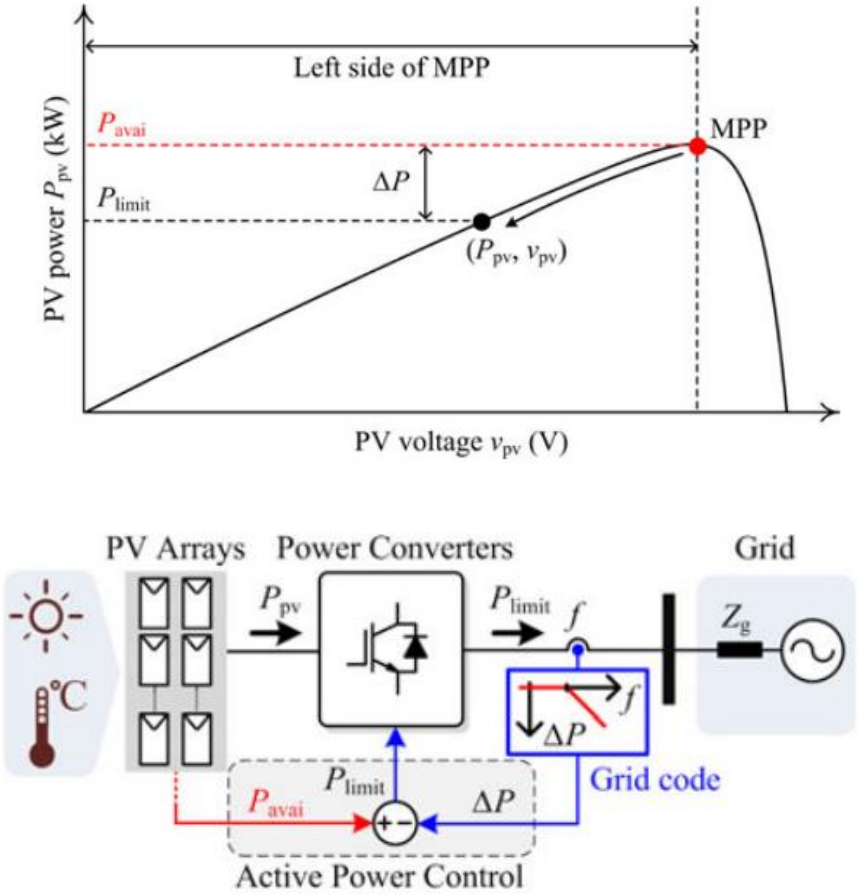

Figure 3.3-1 Active Power Control dynamic and control scheme [5]

- In [4] a constant power generation control is studied. This control is able to rapidly and smoothly transit from MPP to CPG; high performance and stable operation are achieved. The study underline control problems when it is necessary to jump instantaneously from one state to another; most controls loose accuracy, are slow and unstable. To achieve CPG the MPPT algorithm is modified at inverter level. The constant power is set at P_{limit} and when P_{pv} (Panel power) is greater than P_{limit} the output power equals P_{limit}, contrarily P_{pv} equals P_{mpp}. Specifically, a two-stage PV is employed, regulating the output power at the left side of the MPP (CPP-L) in order to avoid stability issues (fast

decrease in power if irradiation changes rapidly) and open-circuit condition, as shown in Figure (3.3.1-2). On the other side working on the left slope slows the tracking of the low power point. Another issue is determined by the voltage step chosen to reach the operating voltage. To track the MPP usually is used the P&O-CPG algorithm which has good performance if irradiation changes are slow (clear day condition, operating at the left side of the maximum power point) but in adverse conditions (cloudy day) it can result in overshoots and power loss. Overshoots happens when the irradiation suddenly increases while power losses happens when irradiation rapidly decreases. To overcome overshoot an adaptive voltage step is used in order to rapidly catch the sudden variation, initially its value will be large but as the difference between P_{limit} and P_{pv} decreases, so the step will. Losses are linked to the iteration steps necessary to reach the new operating point. To reduce the number of iterations the voltage can be approximated to 71-78% of the open circuit voltage and perturb until the MPP is reached; the said procedure called, fractional open circuit voltage, brings the system to zero power production to exactly know the V_{oc} value at a given level of irradiation, it is not clear in the paper if an estimation of V_{oc}, manufacturer value is used or the actual measure at zero power.

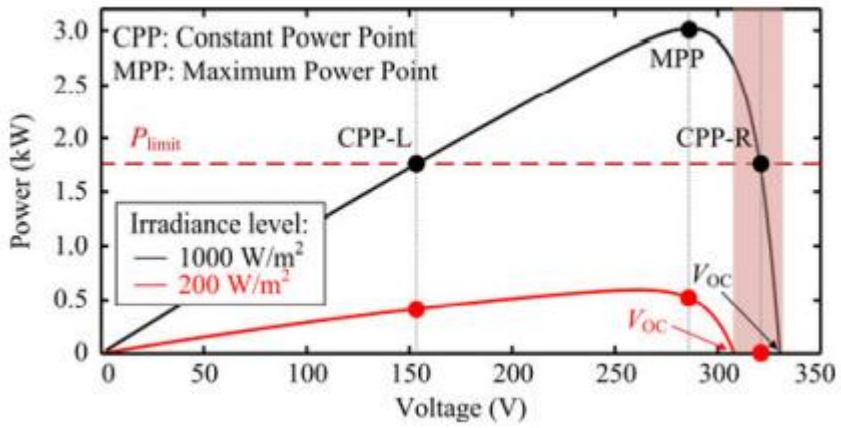

Figure 3.3-2 Stability problem working at MPP' right side [4]

- In [5] the delta power control (DPC) is presented, Figure (3.3.1-1). As for the constant power generation two algorithms are implemented: the MPPT and the CPG. One PV string works and estimates the maximum power (MPP) while other strings regulate the PV power to reserve a delta of power to readjust frequency deviation. The Delta power constraint (also called Power Reserve Control) is currently used in large-scale power plants. As PV propagation is still growing this kind of control is expected to be applied to medium and small-

scale systems. The pressing issue is estimating the available power, the P_{limit} is set consequentially, using irradiance could be a solution but it needs an accurate estimation, hence more costly. Therefore, this solution is not available for residential and small-scale systems. A quadratic approximation curve-fitting fit the purpose, specific as it is model-based and approximated. The available power is estimated without irradiance, one of the PV module strings will work at MPP so it is possible to retrieve the power simply multiplying the number of strings with the power of the MPP string, Equation (3.3.1-1). Of course, this is an estimation which depends by the MPPT algorithm accuracy and it is not suitable for larger system where more than one string is operated at MPP, the available power will be an average, another issue in large system is the modules spatial distribution, meaning that different levels of irradiance could reach different modules at different positions, making available power estimation not accurate. The slaves must work at CPG at the left side of P-V characteristic due to stability problems mentioned and illustrated in Figure (3.3.1-2). The DPC differs from CPG because the power limit changes as the MPP changes to achieve the delta constraint, Equation (3.3.1-1).

$$P_{avail} = n \cdot P_{mpp} \tag{3.3.1-1}$$

$$P_{pv} = P_{avail} - \Delta P \tag{3.3.1-2}$$

P_{pv} is the system power, P_{avail} is the maximum available power, n is the total number of PV strings of the system and ΔP is the power reserve, function of the grid frequency.

- In [6] a pseudo power point tracking provides frequency regulation to the photovoltaic system. Following a Δf there is a ΔP. To countermeasure frequency deviation inside the MPPT controller (Inverter control) two algorithms are coded: the P&O (Perturb and Observe) and the modified fractional V_{oc} method, the latter control the duty cycle of the boost converter to keep the DC bus voltage constant. Conventionally the MPP voltage is a fraction of the V_{oc}, given by the proportionality factor k (0.71-0.78 when tracking the maximum power, 0.8-0.95 when using the modified algorithm). There are some disadvantages in this approach, first Voc needs to be known then based on its value the MPP is individuated and finally the ratio k is used to lower the operational voltage. But knowing V_{oc} means shut down the PV system and restart it for as many times it necessary to work at reduced power and k is choice made the control works at the right side of MPP. The trigger is an external frequency signal fed to the control. The pros are its simplicity, the fast response

with short transitory and the possibility of a power margin under vary condition of insolation.

- In [7] the control implemented respond to both slow and fast frequency deviation, the power-frequency droop can change power as consequence of a Δf, P-f characteristic, without interference between switching from one control to the other. Three controls are studied in the same control system:
  1. Power output curtailment control; the panel works at P_0, its value is less than P_{mpp} so that their difference is a power reserve able to compensate frequency deviations. The P_{mpp} is retrieved using additional modules with same I-V, compute Isc and estimate P_{mpp}. P_{mpp} is proportional to I_{sc}.
     This estimation is less accurate as change in current are rapid as changes in irradiation.
  2. From the P-f droop control the active power is computed, P_0 is adjusted according to the droop setting in slow frequency variation, variations within regulation limits so that frequency returns to the nominal value. When frequency variation exceed regulation limits the control use the fast frequency droop characteristic.
     Both the droops don't interfere with each other (voltage cycles observation) as illustrated in Figure (3.3.1-3) and to avoid discontinuity in the droop setting, Equation (3.3.1-3), the same slope is used.
     $$\frac{f}{P} = -\frac{4\%}{P_{mpp}} \qquad (3.3.1\text{-}3)$$
  3. Reactive power control using Q-V droop control, the inverter injects reactive power to compensate voltage variations.

This control is validated by a simulation which shows the independence of slow and fast controls.

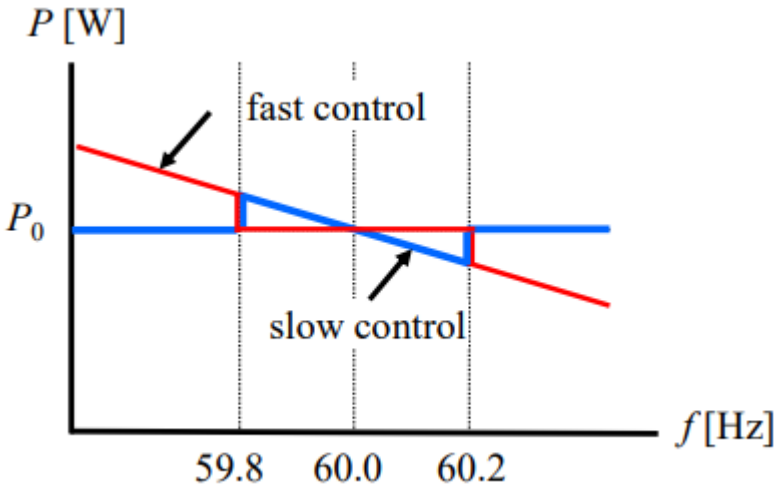

Figure 3.3-3 *P-f* droop control study characteristic [7]

- In [8] a two-stage control is implemented to work accurately under dynamic conditions. The DC/DC converter usually works at MPP, but in this study the control is more complex. The control system is dived in four sub systems.
  1. Continuous estimation of MPP thanks to high pattern recognition of ANN. ANN takes as input G and T and returns as output V_{mpp} and P_{mpp}. V_{mpp} is needed to determine the deloading zone. The neural network is trained with many datasets among which its 30% is reserved for validation and testing.
  2. Reserve Generation Algorithm (RGA) is used to deload, the deloading region is at the right side of the MPP, $V_{mpp} < V_{pv} < V_{oc}$. V_{pv} is checked and if its beyond the right zone limits the V_{ref} is perturbed with a voltage step, dV_1. To trace P_{ref} it is compared to P_{pv}.

     $P_{ref} > P_{pv}$>, V_{ref} is decreased by dV_2 (dV_1>dV_2)

     $P_{ref} < P_{pv}$, else

     This continues until $P_{ref} = P_{pv}$.
  3. Active power reserve is estimated with a fuzzy logic. Simple and good at handling non-linearities. Inputs are G and T_{dev} (Temperature deviation from the STC), the output is the percentage reserve r. The reserve is inputted into the droop control, when G(STC) and $T_{dev} = 0$, r is equal to 20% (max allowed reserve) while when G is low and T_{dev} is high r is at 0%.
  4. The droop control compute P_{ref} for RGA, Equation (3.3.1-4)

$$P_{ref} = P_{mpp}[1 - (r + k\Delta f)] \tag{3.3.1-4}$$

Δf is the frequency deviation and k is a gain constant and depends by the droop characteristic, Equation (3.3.1-5).

$$k = 100 \cdot \left[\frac{f_n - f_{min}}{P_{ref}^{r=0.2} - P_{ref}^{r=0}} \right] \quad (3.3.1\text{-}5)$$

This method enables the inertial PV capability and handle well power reserve techniques issues. In this study the partial shading condition is not compelled. Although efficient this solution is costly, ANN and fuzzy control require many data and processing. Accuracy depends on the value chosen for k since Equation (3.3.1-5) gives a range of values.

4. Development of a Model-Based Algorithm for Power Reduction

In this chapter will be presented an algorithm for a PV system able to work at reduced power without the need to switch operating point between the MPP and the point at reduced power. This is a great advantage as power peaks and transitory are avoided along with the equipment needed to diminish them and absorb the surplus power, resulting more economic and efficient.

The control strategy chosen derives from a model based maximum power point tracking algorithm (MB MPPT) [1]. This solution guarantees high efficiency during steady state conditions and fast dynamic, with improved performance during rapid changes of weather inputs if compared to other popular algorithms [3]. A MB MPPT considers the model of the PV panel with its weather inputs, temperature and irradiation. The model is visually translated into I-V characteristic which change with temperature and irradiation.

The model predicts the voltage to be fed to the power converter. The model proposed does not need any irradiation measurement which lower the cost and has only four unknown parameters which are estimated with OLS or WLS, the identification of the voltage is done iteratively but with fast convergence. The efficiency of the MPPT depends on how quickly the power converter can follow the MPP. The aim is to estimate iteratively V_{mpp} and I_{mpp}, Equations (4.1-4.2), knowing the PV model a priori, voltage estimation is chosen to track MPP since is temperature dependent with little to none dependence from irradiation, hence it presents a slower dynamic than current. Irradiation measurement instruments are expensive and may not work optimally if soiling covers their surface.

$$V_{mpp} = V_{mpp}\left[1 + \beta_{mpp}(T - T_0) + \delta_1 \ln\left(\frac{G}{G_0}\right) + \delta_2 \ln^2\left(\frac{G}{G_0}\right)\right] \quad (4.1)$$

$$I_{mpp} = I_{mpp0} \cdot \frac{G}{G_0}\left[1 + \alpha_{mpp}(T - T_0)\right] \quad (4.2)$$

G_0 and T_0 are irradiation and temperature at STC. Irradiation knowledge is avoided rearranging Equation (4.2), not considering the proportion with temperature leading to Equation (4.3), this result is substituted into Equation (4.1) leading to Equation (4.4).

$$\frac{I_{mpp}}{I_{mpp0}} \cong \frac{G}{G_0} \quad (4.3)$$

Equation (4.3) is accurate only when the actual value of I_{mp} is adopted yet a proper value of voltage can be obtained only with temperature knowledge, leading to a better estimation of current. Then again, using the measured current value leads to a better value of voltage and so on. When Equation (4.5) and Equation (4.4) results get close to each other. Finally, the model is achieved and characterized by only four parameters.

$$V_{mpp} \cong V_{mpp0}\left[1 + \beta_{mpp}(T - T_0) + \delta_1 \ln\left(\frac{I}{I_{mpp0}}\right) + \delta_2 \ln^2\left(\frac{I}{I_{mpp0}}\right)\right] \quad (4.4)$$

$$V_{mpp} \cong V_{mpp0}\left[1 + \beta_{mpp}(T - T_0) + \delta_1 \ln\left(\frac{I_{mpp}}{I_{mpp0}}\right) + \delta_2 \ln^2\left(\frac{I_{mpp}}{I_{mpp0}}\right)\right] \quad (4.5)$$

$$V_{mpp} = A_0 + A_1 T + A_2 \ln\left(\frac{I}{I_{mpp0}}\right) + A_3 \ln^2\left(\frac{I}{I_{mpp0}}\right) \quad (4.5)$$

Parameters are estimated with OLS but it is found that WSL method is more robust and optimal as is less affected by partial shading and results in less system losses [4]. Parameters also depend on combination of G and T. External inputs influence heavily the final error on power production that is why in the algorithm parameters are updated on monthly basis and computed on clear days [5].

Iterations to retrieve V_{MPP} are not complex and a simple model is preferred over a complex one.

This same model is now modified in order to work at reduced power, a level of power which is less than the MPP. The user choses the power percentage at which the PV module has to work and consequently Equation (4.5) is modified in Equation (4.6) or synthetically in Equation (4.7).

$$V_{\%} \cong S_V \cdot \left[A_0 + A_1 \cdot T + A_2 \ln\left(\frac{I_{\%}}{S_I}\right) + A_3 \ln^2\left(\frac{I_{\%}}{S_I}\right)\right] \tag{4.6}$$

$$V_{\%} = S_V \cdot V_{mpp} \tag{4.7}$$

$$I_{\%} = S_I \cdot I_{mpp} \tag{4.8}$$

$V_{\%}$ is the voltage reduced by the power percent, S_V is the voltage scale factor and its value should be close to the power percent applied. For current, Equation (4.8), $I_{\%}$ value will be in between I_{sc} and I_{mpp}, S_I is close to 1.

Considering a single P-V curve, firstly the MPP is found with a quadratic interpolator (V_{mpp}, I_{mpp}) then, working at the left side of the P-V characteristic for stability reasons, the point with minimum difference between voltage vector product with current vector and the percentage of power reduction times the product of V_{mpp} and I_{mpp} is found. Through Equation (4.7) and Equation (4.8) S_V and S_I are obtained. The same procedure is repeated for every daily curve.

4.1 Data Processing

From now on the aim is to reduce the error of the algorithm output in boundaries ±2.5. To do so it is necessary to start from the data measured and call out every detail that could lead to the final error exceeding the set limits.

4.1.1 Data set

The algorithm is coded with MATLAB, during the year 2017 each day, through an experimental setup described in [2], from 6190 up to 10350 I-V curves were recorded during the day at varying temperature (0-60 °C) and irradiation conditions (200-1400 W/m²). Then for each curve the V_{mpp} and I_{mpp} are obtained through a quadratic interpolator. Other environmental data were registered such as RH and T_{amb}. All curves are filtered from noise. Two panels are connected to the equipment; panel 'grande' and panel 'piccolo', they differ from each other for different electrical characteristic values. In Table (4.1-1) are listed the characteristic of the panel considered.

Panel 'grande'	
P_r [W]	180
I_{SC} [A]	5
V_{OC} [V]	40
Cell type	mc-Si

Table 4.1-1 Panel manufacturer data

4.1.2 Incomplete data, Partial shaded curves and technical constraints

The data set contains thousands of I-V curves out of which some present some bad data. To acquire an I-V curve a voltage ramp starting from zero to 40 V is used but sometimes the acquisition starts after zero resulting in a partial ramp devoid of the initial part, which could create problems with the power tracking algorithm. Examples found in the data are:

1. Voltage ramp starts after the percentage of the MPP set, the P% is not present, the algorithm will take the minimum point at the left side of the curve.

2. Partial shade drops on the I-V curve translate into peaks on the P-V thus the algorithm will consider the first local maximum as MPP and the percentage power will be at its left side

For the first point every curve whose voltage started after 5 V is erased.

The MB MPPT algorithm works well when considering close to ideal I-V curves, anything related to undesired effects related to partial shading must be individuated. Partial shading happens when a shadow is cast on the panel surface, it can be a passing cloud or nearby objects, obstacles even an operator shadow. Evidence of this event is graphically shown on the I-V curve. Partial shading manifest with steps and notches but there can be other causes to this shape like when the by-pass diode is short circuited or a cell is damaged. The cell current is reduced, reducing also the maximum current produced by other cells in series. By-pass diodes are useful to avoid the reverse bias of the section excluded. Avoiding partial shaded characteristics helps the algorithm. In case of partial shading the P-V characteristic will present more than one peak, many local maxima deceive the algorithm; both the MPP and the point at reduced power belong to the first peak found which may not be the actual peak corresponding to the knee on the I-V curve. The algorithm is implemented on both clear and casted days, where irradiation rapidly varies. But the algorithm solely depends on temperature as weather input with slower variations.

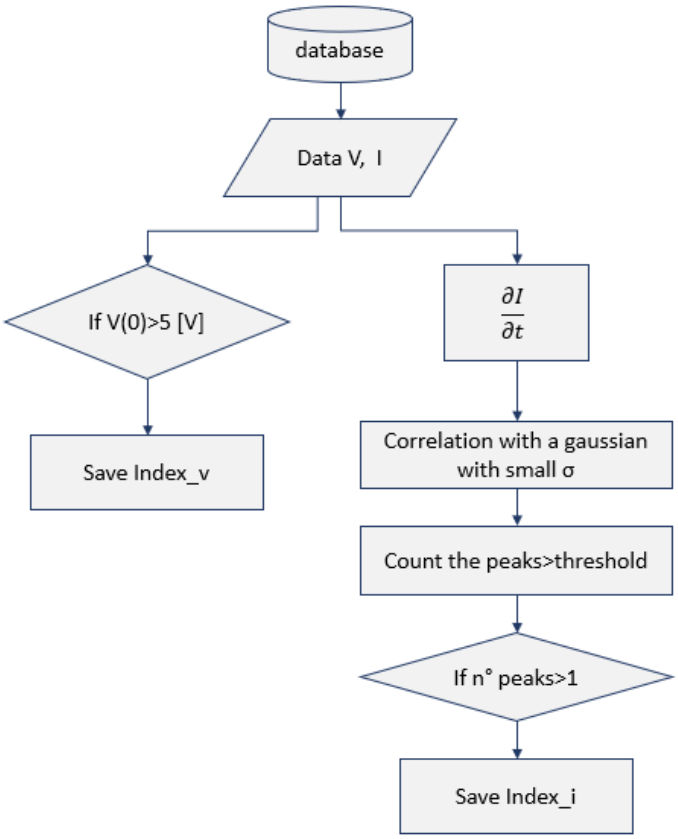

Figure 4.1-1 Block diagram of voltage ramp and partial shading algorithm

In Figure (4.1.2-1) the block diagram of the algorithm able to detect partial shaded curves and curves with a voltage ramp starting after 5 V, detection means getting the indexes (Index_v and Index_i) and store them in order to use them or not.

The algorithm works computing the derivative of the current, in case of shading the derivative plot will present more than one peak (in a clear curve the peak is due to the knee, located at MPP, in case of shading there will be more knees, hence more peaks-change of angular coefficient), then the derivative is correlated to a gaussian curve with set mean and standard deviation so that the peaks can be detected, if they exceed a threshold, and counted; finally, the algorithm save the curve which is affected by partial shading if the number of peaks exceeds one.

The algorithm is quite immediate yet it is not precise and it is data dependent. Given the set of data collected for this scope a certain value of mean and especially standard deviation are chosen and also the value of the threshold. Different values of standard deviation are implemented to see the total number of deleted curves, the curves effectively affected by partial shading, the curves detected but not affected by partial

shading and the curves not detected but affected by partial shading. In Table (4.1.2-1) there is a year summary of the said quantities with relative percentages.

sigma	right detected	%	wrong detected	%	tot detected	not detected
0,05	456	100%	2	0%	458	124
0,08	543	99%	6	1%	549	62
0,1	557	97%	17	3%	574	44
0,15	537	91%	55	9%	592	58
0,2	533	78%	148	22%	681	73
0,25	523	63%	307	37%	830	82
0,3	512	52%	471	48%	983	100

Table 4.1-2 Summarizing Table of Sigma and curve

The table shows how a reduced sigma is better at detecting partial shaded curves and reduce false positives, moreover the curves not detected are less.

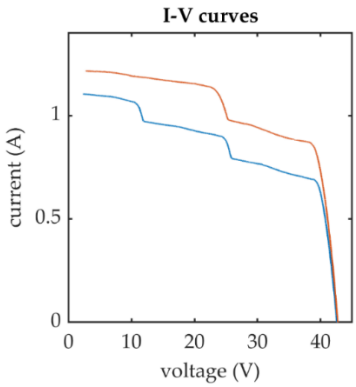

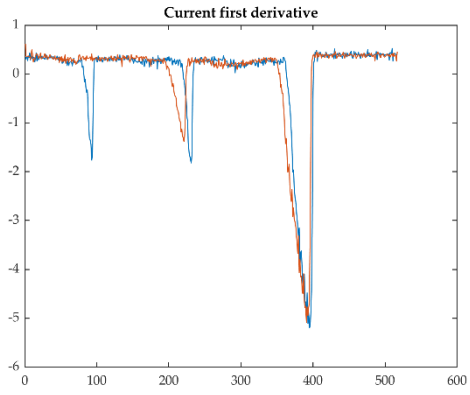

a) σ=0.05, curves wrongly detected=0, curves not detected=1

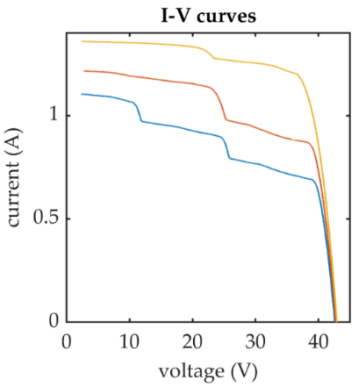

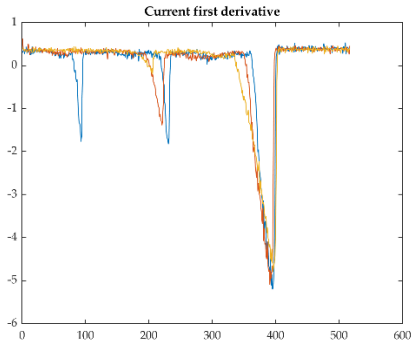

b) σ=0.08, curves wrongly detected=0

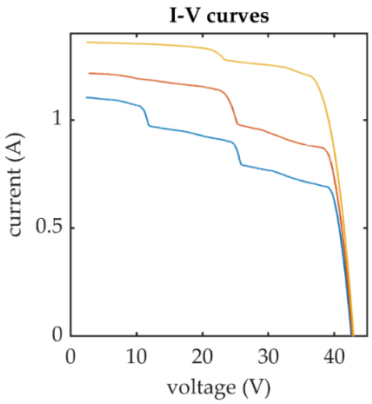

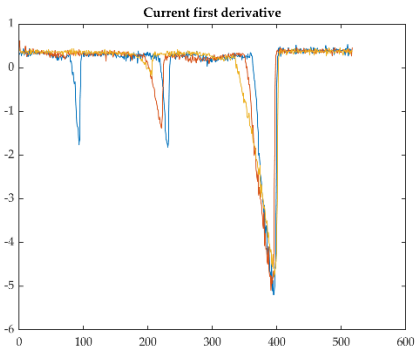

c) σ=0.1, curves wrongly detected=0

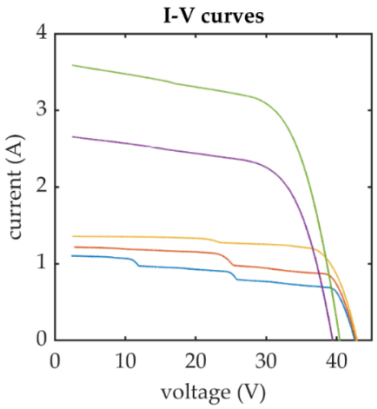

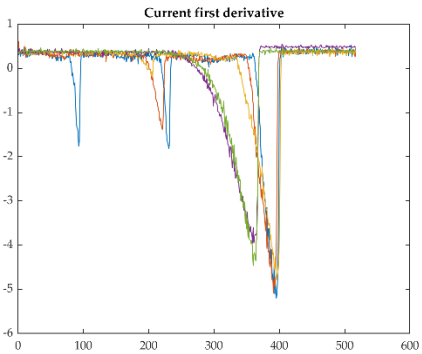

d) σ=0.15, curves wrongly detected=2

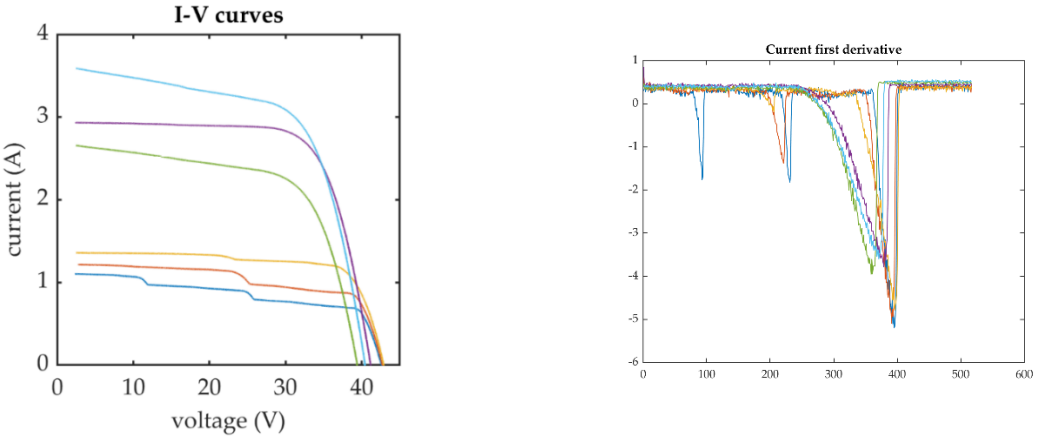

e) σ=0.2, curves wrongly detected=3

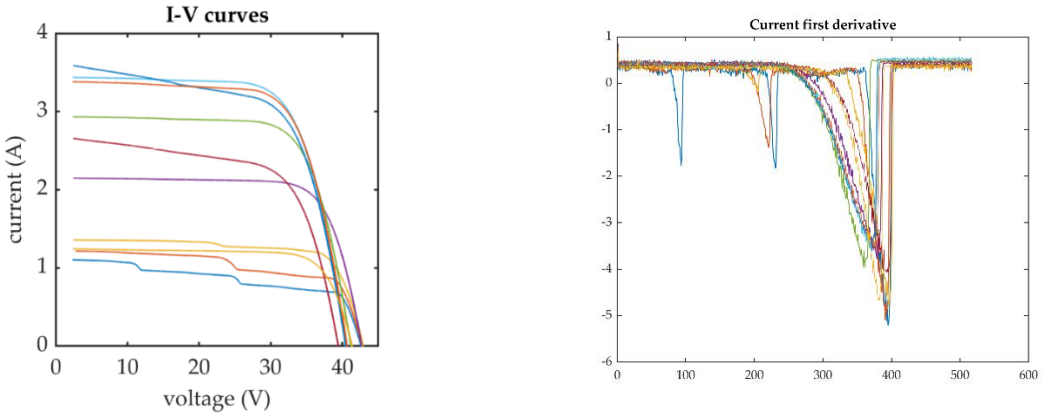

f) σ=0.25, curves wrongly detected=7

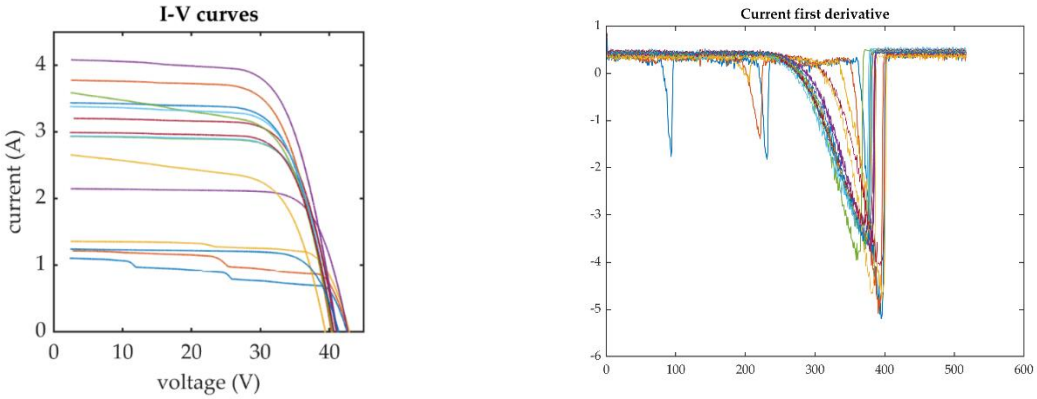

g) σ=0.3, curves wrongly detected=11

Figure 4.1-2 Partial shaded curves detection algorithm example with different sigma. Shaded I-V curves on the left and first derivative of the current on the right

In Figure (4.1.2-2) comparing the figures (a-g), it can be noted that as sigma grows the algorithm wrongly detect I-V curves which are not affected by partial shading, the curves are in the near proximity of the shading interval but are unaffected by the phenomenon. The algorithm gets better as sigma value is lowered, from σ=0.10 there are no more wrong detected curves. Even if the algorithm is better at low sigma, it doesn't perfectly detect all shaded curve as it can be seen in the Table (4.1.2-1), for σ=0.15 the curves not detected are 58, still high. Considering σ=0.10 the situation is much better, the number of wrong detected curves decreases along with the curves not detected, among which almost the totality of them presents an effect of partial shading almost negligible. Further decreasing of sigma visually bring the same results of σ=0.10 if σ=0.08 is considered, though looking at Table (4.1.2-1) the number of not detected curves increase. A further decrease (a) does not detect a shaded curve and again the number of not detected curves increases. A good compromise is σ=0.10, most curves are detected with respect to others sigma.

To be noted that some curves were not counted in the wrong not detected although they do not follow the 'ideal' shape of an I-V curve. Curves with an ascending slope and a decreasing slope, making the MPP position higher than the I_{sc} were spotted. Other curves showed small though visible oscillations.

Now the relations between S_V and T and S_I and G are depicted in Figure (4.1.2-3) without and with deletion of curves with either Index_v and Index_i.

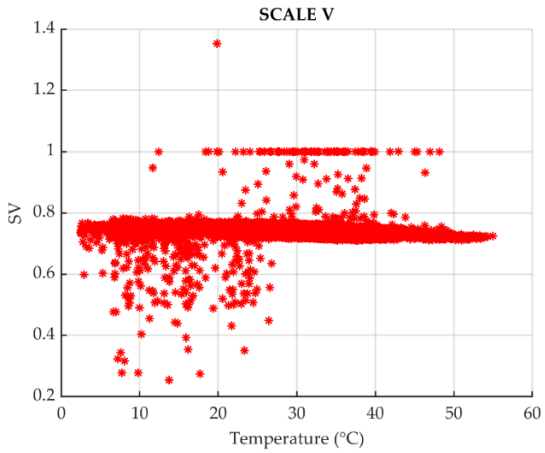

(a) SV-T relation of all data

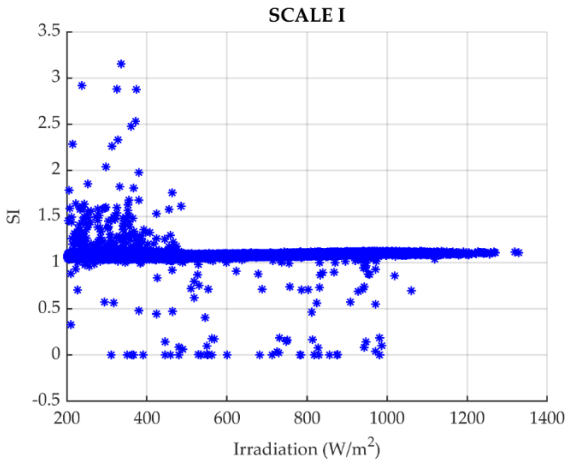

(c) SI-G for all data

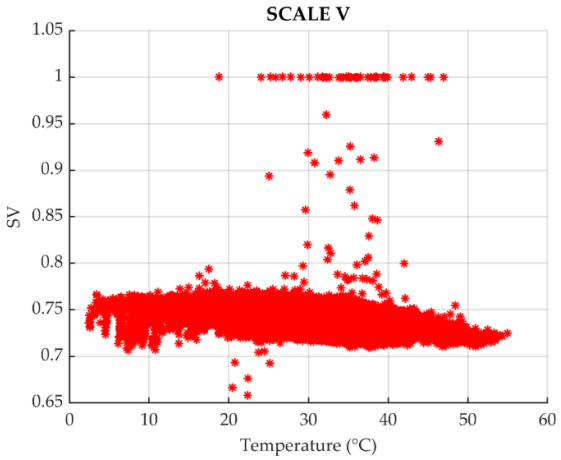

(b) SV-T relation without considering detected indexes for σ=0.1

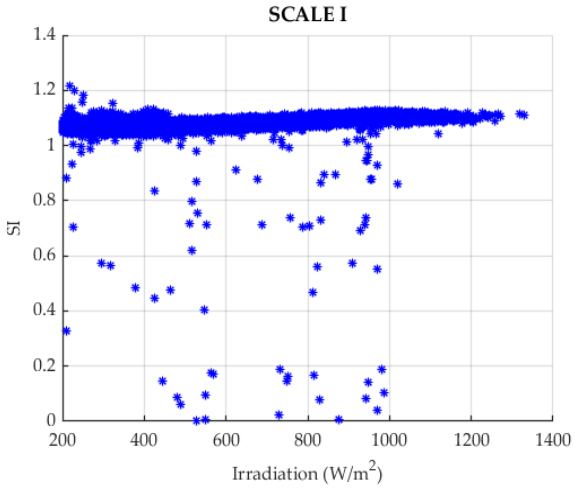

(d) SV-T relation without considering detected indexes for σ=0.1

Figure 4.1-3 SV-T and SI-G relations

Comparing Figure (4.1.2-3) (a) and (b) a drastic change is seen as voltage scale factors less than 0.65 are 'erased' from the algorithm and so are the corresponding points on (c) resulting in (d). as predictable partial shading happens at low temperatures and low levels of solar irradiation. But what causes a small S_I? And S_V close to 1?

Even though there's an amelioration some scale factors values are still not acceptable; yet it was found that the remaining small value of SI correspond to I-V curves showing a good shape. So, a further study was implemented on these points in order to explain scale factors values. The I-V curves which were not eliminated by the partial shading algorithm but had deranged value of scale factors present indeed a good shape, close

to the ideal one, but further analysis showed, plotting on the same curve the coordinates of MPP, V_{mp} and I_{mp} obtained through a quadratic interpolation, a mismatch. In fact, the point was not plotted on the curve but far from it to a certain degree, for further confirmation even the P-V curves and the P_{mpp} was plotted, a couple of examples are reported in Figure (4.1.2-4).

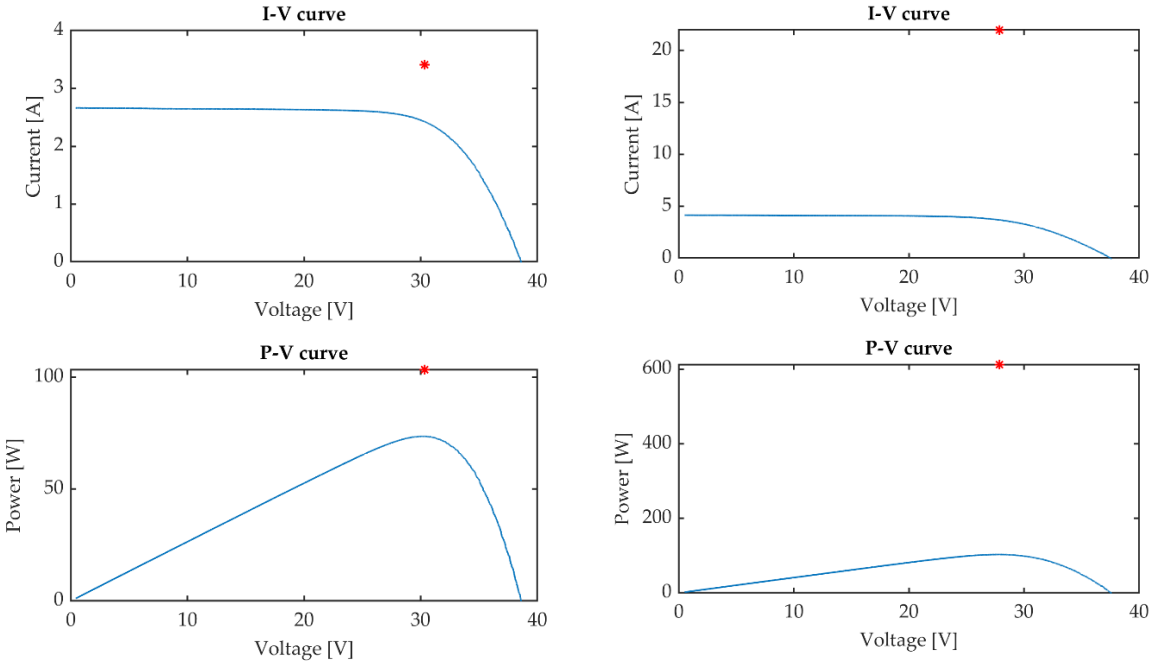

Figure 4.1-4 I-V and P-V curves with MPP, interpolation error

Therefore, the quadratic interpolator was changed.

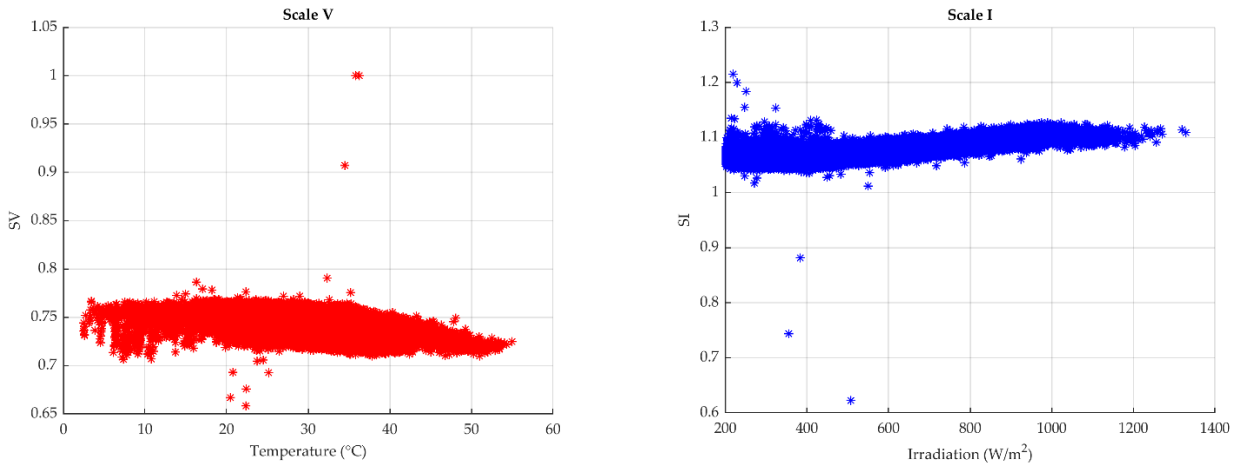

Figure 4.1-5 Scale factors with new interpolator, without partial shading

Comparing Figure (4.1.3-4(a) and (b)) with the corresponding in Figure (4.1.2-5) it can be seen that the new interpolator works better than the previous one and problematic points get erased, from around 65 bad data only 3 bad data points remain. The new plot shows clearly the effectiveness of the partial shading algorithm combined with a more refined interpolator, focus can be made on the less dispersive data points with a mean S_V of 0.74 and a mean S_I of 1.08. Points of S_V closer to 1 and S_I below one corresponds to each other and are due to interpolation error.

4.2 Error

The relative error between the algorithm prediction, $P_{mpp\_\%P}$, and the actual value scale by a power percent, $\%P \cdot P_{mpp}$, is performed, Equation (4.2-1).

$$e = \left(P_{mpp\_\%P} - \%P \cdot P_{mpp}\right) / P_r \cdot 100 \qquad (4.2\text{-}1)$$

The aim is to ascertain that the error falls inside the limits defined by the European normative, set to ±2.5% of the nominal power, in order to connect the PV system to the electrical grid and fulfill the requirements for frequency regulation, curtailment mode [6]. The error is plotted with the following constraints:

- Voltage ramps; Index_v
- Partial shading; Index_i
- Manufacturer constraints

Manufacturer constraints refer to values of power voltage and current peculiar to the PV module. The rated power is of 180 W, the short circuit current is 5.24 A, the short circuit voltage is 40 V. Any values higher than the rated ones the error point would be erased. So are curve indexes corresponding to Index_i and Index_v.

In Figure (4.2-1) the final error is plotted before and after constraints applying actual values of S_V and S_I. In (a) positive error is quite high but only few points are affected whilst negative error is more frequent but less impacting. In (b) the situation improves mainly on the positive side, negative error remains unaltered.

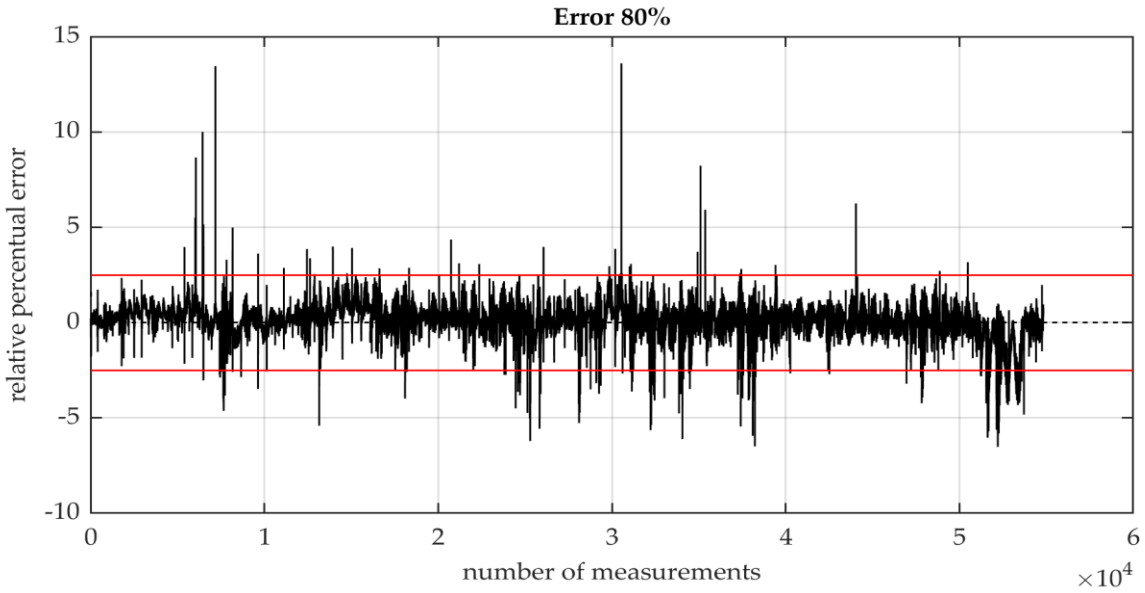

(a) Relative error of all data

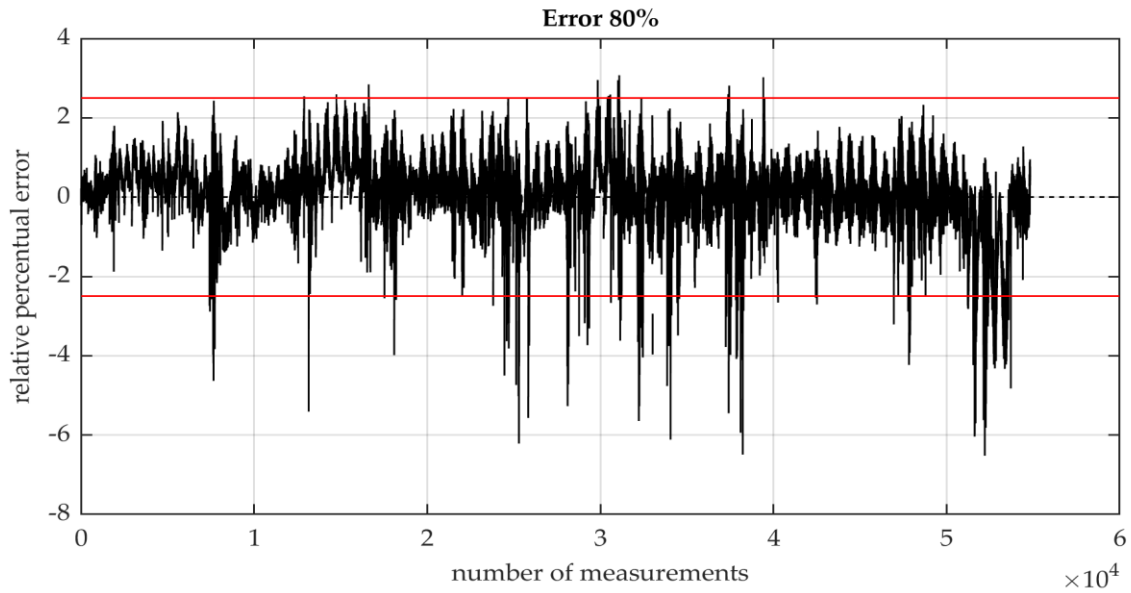

(b) Relative error with constraints, actual SV and SI

Figure 4.2-1 Effect of constraints on the relative error comparing a) and b)

Now a statistic process is being perform on the error. Before anything, values which are infinite or not a number are erased. The error histogram is built.

	Err 80%	Err 80% filtered
Erased NaN or Inf	792	1619
max	13.5968	3.0743
min	-6.5212	-6.5212
Range	20.1179	9.5955
μ	0.1319	0.1325
σ	0.7798	0.7643
Mode	0.1830	0.2480
Median	0.1978	0.2002
Skewness index	-1.3111	-1.7499
Kurtosis index	14.5526	10.8212

Table 4.2-1 statistic table

In Table (4.2-1) are grouped statistical data belonging to the error before and after constraints, both considering the actual values of scale factors. The range, difference between the max and min, has decreased considerably. The mean has slightly increased while standard deviation has slightly decreased. The mean depends by outliers, histogram tail values. In both cases the skewness index is negative meaning the distribution is not symmetric, but it spreads to the left, the value is greater than one in both cases, in the second case the higher value is due to error data deleted. The kurtosis index is reduced in the second case but far from the normal distribution, outliers' weight is still relevant. In Figure (4.2-2) the relative histogram is reported. σ is relatively small, indicating that most of points do not differs much from μ, which is the arithmetic mean, highly dependent on outlier points (since every result is weighted the same). Given the highly asymmetric distribution the median is a better indicator to consider for the centering, less dependent by outliers. Another statistic index which gives important information is the mode, center value of the highest frequency class bin. The mode is the most popular value in the distribution and although not zero it is quite small.

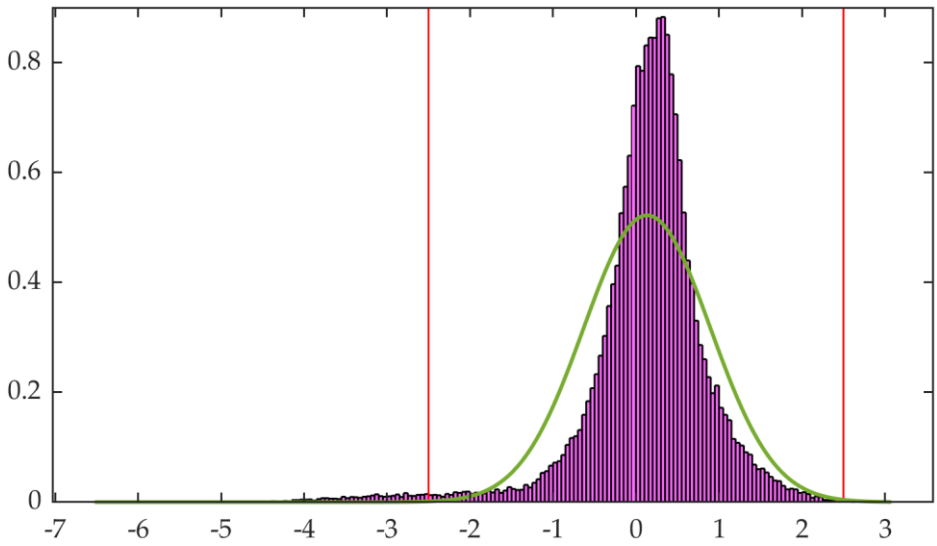

Figure 4.2-2 histogram with fitted normal distribution

Correlation between normal distribution fit to the error data (green curve in Figure (4.2-2)) and data distribution through Pearson correlation, Matrix (4.2-1), the value R ranges between -1 to +1, when R is close to ±1 there is a strong correlation but when R is close to 0 there is no correlation. In matrix (4.2-1) the values on the diagonal are self-correlated while the off-diagonal elements give the correlation between the error distribution and the fitted distribution, given by the ratio of the covariance between the distributions and the product of their respective standard deviations.

$$\begin{matrix} \text{R-value} \\ \begin{bmatrix} 1 & 0.2511 \\ 0.2511 & 1 \end{bmatrix} \end{matrix} \tag{4.2-1}$$

0.2511 is a low positive correlation. Meaning that the normal distribution does not represent the error distribution. Considering the absolute value of the error positive distribution were fitted, Figure (4.2-3) yet results in Table (4.2-2) show that none of the distributions possesses a high R-value meaning the correlation is not high enough to choose the distribution.

Fitted distribution	R-value
Normal	-0.4401
Exponential	-03673
Lognormal	-0.3290
Logistic	-0.3884
Extreme values	-0.5286

Table 4.2-2 R value of fitted distributions

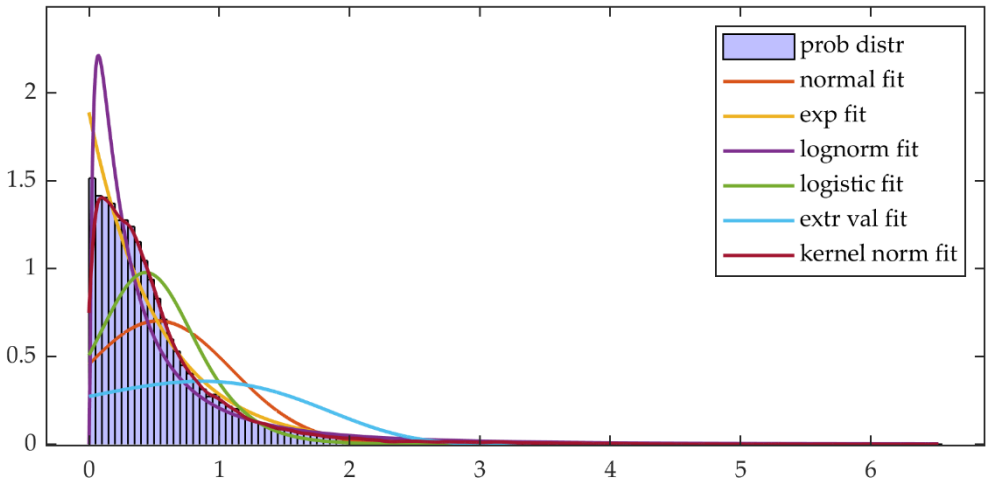

Figure 4.2-3 absolute error distribution fit with positive distributions

Statistical model of the error can be seen as a quality process on validation therefore the natural tolerance, six-sigma, can be used to set the limits and see if the error follows the normative. Even if the distribution fit does not result in a normal fit, the assumption is that the error does follow a normal distribution. As the number of samples is very high k=3, for any Q. The lower and upper limits of error are [μ-3·σ=-2.1604, μ+3·σ =+2.4254] both inside the regulation [-2.5, -2.5]. Only roughly 2% of points are outside the six sigma lower and upper natural tolerance limits.

The error distribution may not follow the normal distribution due to the fact that not every day is a clear sky. Clear sky is important when implementing the MB-MPPT algorithm as it is most efficient when this condition is available. The partial shading

phenomenon can indeed bring some disturbances but it was constrained in particular time instants of the day and considering the total amount of data points acquired it only affect a small portion of them. Other sources may lay in the panel soiling, a reversible effect, which change the shape of the I-V curve working at lower intended power and consequentially could explain the lower value of S_V noted. From a theoretical of 0.8 to a mean of 0.74. Another reason always in line with the same principle describe for soiling, is the degradation of the panel. Degrade changes the panel electrical parameters in time changing the shape of the I-V curve, so the algorithm model may not coincide anymore with the actual model of the panel. Corrective actions such recalibration and re-estimation of the model parameters can dampen this problem. Particularly, it could be useful knowing beforehand when there will be a substantial power loss in order to update the algorithm model, for such reason degradation modes individuation and degradation rates computation can contribute to error reduction.

5. Conclusion

The purpose of this thesis is studying and including degradation effects in a PV system reliability and highlight the many challenges and variables participating in the overall loss of performance. Power loss and decay in time are important in the optic of power reserve to actively contribute to grid frequency deviation in case of photovoltaic systems connected to the grid. Usually, the performance index used to visualize degradation is the normalize maximum power output that, if decreased, the system power reserve could be insufficient for the regulation purpose aside risk of generators disconnection. The model-based algorithm to reduce power possesses intrinsically degradation information, in the daily shape of the I-V characteristic and in the parameter estimates. These coefficients strongly depend on the daily curves acquired, curve which change with weather inputs, not only seasonally changing but also in the operational years the system is on. Changing parameters of the I-V curve can be linked to degradation modes and when a substantial power loss is observed the algorithm itself must be revisited and updated. But this part is left for future development.

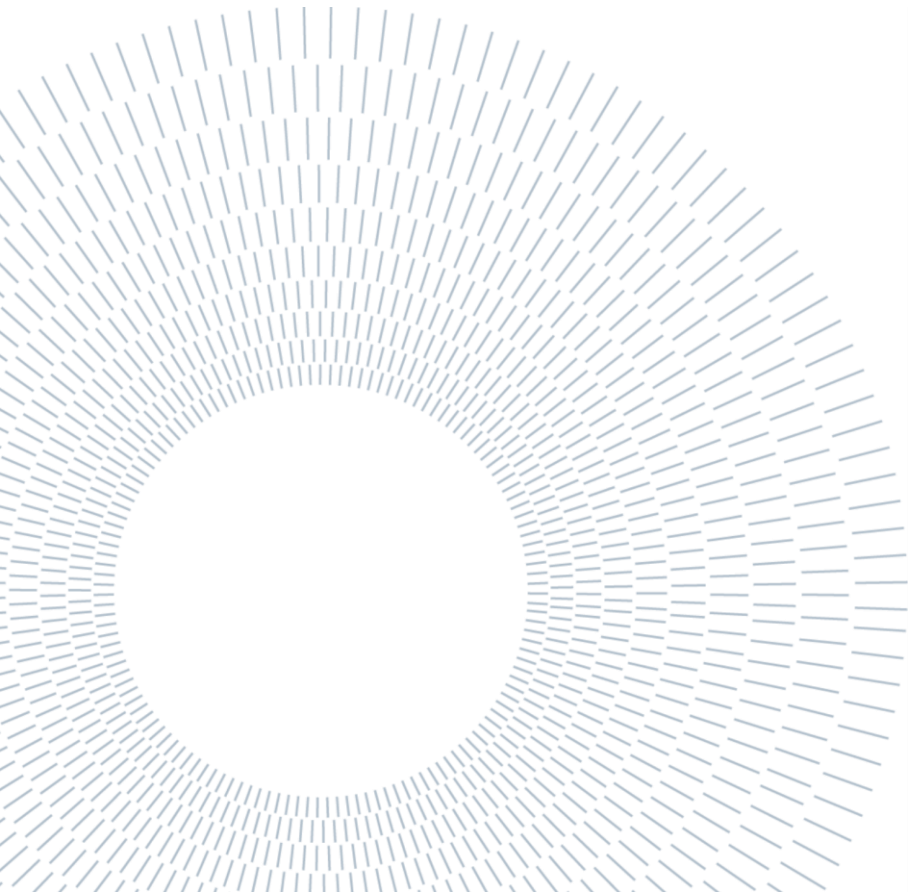

Bibliography

Chapter 1

[1] P. Hersh, K. Zweibel, Basic Photovoltiac principleas and methods, Midwest research institute, U.S Department of Energy, February 1982.

[2] M. Köntges, G. Oreski, U. Jahn, M. Herz, P. Hacke, K.A. Weiss, G. Razongles, M. Paggi, D. Parlevliet, T. Tanahashi, Roger H. French, Assessment of Photovoltaic Module Failures in the Field, IEA PVPS Task 13, May 2017.

[3] Web resource: pv magazine International – Photovoltaic Markets and Technology (pv-magazine.com)

Chapter 2

[1] Vázquez, M. and Rey-Stolle, I. (2008), Photovoltaic module reliability model based on field degradation studies. Prog. Photovolt: Res. Appl., 16: 419-433. https://doi.org/10.1002/pip.825

[2] Vikrant Sharma, S.S. Chandel, Performance and degradation analysis for long term reliability of solar photovoltaic systems: A review, Renewable and Sustainable Energy Reviews, Volume 27, 2013, Pages 753-767, ISSN 1364-0321, https://doi.org/10.1016/j.rser.2013.07.046.

[3] S. Lindig, I. Kaaya, K. Weiss, D. Moser and M. Topic, "Review of Statistical and Analytical Degradation Models for Photovoltaic Modules and Systems as Well as Related Improvements," in IEEE Journal of Photovoltaics, vol. 8, no. 6, pp. 1773-1786, Nov. 2018, doi: 10.1109/JPHOTOV.2018.2870532.

[4] Jordan, Dirk & Silverman, Timothy & Wohlgemuth, John & Kurtz, Sarah & VanSant, Kaitlyn. (2017). Photovoltaic failure and degradation modes: PV failure and degradation modes. Progress in Photovoltaics: Research and Applications. 25. 10.1002/pip.2866.

[5] Pramod Rajput, Maria Malvoni, Nallapaneni Manoj Kumar, O.S. Sastry, G.N. Tiwari, Risk priority number for understanding the severity of photovoltaic failure modes and their impacts on performance degradation, Case Studies in Thermal

Engineering, Volume 16, 2019, 100563, ISSN 2214-157X, https://doi.org/10.1016/j.csite.2019.100563.

[6] M. Halwachs, L. Neumaier, N. Vollert, L. Maul, S. Dimitriadis, Y. Voronko, G.C. Eder, A. Omazic, W. Mühleisen, Ch. Hirschl, M. Schwark, K.A. Berger, R. Ebner, Statistical evaluation of PV system performance and failure data among different climate zones, Renewable Energy, Volume 139, 2019, Pages 1040-1060, ISSN 0960-1481, https://doi.org/10.1016/j.renene.2019.02.135.

[7] I. Kaaya, M. Koehl, A. P. Mehilli, S. de Cardona Mariano and K. A. Weiss, "Modeling Outdoor Service Lifetime Prediction of PV Modules: Effects of Combined Climatic Stressors on PV Module Power Degradation," in IEEE Journal of Photovoltaics, vol. 9, no. 4, pp. 1105-1112, July 2019, doi: 10.1109/JPHOTOV.2019.2916197.

[8] Ismail, Kaaya & Ascencio-Vasquez, Julian & Weiss, Karl-Anders & Topic, Marko. (2021). Assessment of uncertainties and variations in PV modules degradation rates and lifetime predictions using physical models. Solar Energy. 218. 354-367. 10.1016/j.solener.2021.01.071.

[9] Escobar, Luis & Meeker, William. (2007). A Review of Accelerated Test Models. Statistical Science. 21. 10.1214/088342306000000321.

[10] Braisaz, Benoit & Duchayne, Chloé & Van Iseghem, Mike & Khalid, Radouane. (2014). PV aging model applied to several meteorological conditions.

[11] Ababacar Ndiaye, Abdérafi Charki, Abdessamad Kobi, Cheikh M.F. Kébé, Pape A. Ndiaye, Vincent Sambou, Degradations of silicon photovoltaic modules: A literature review, Solar Energy, Volume 96, 2013, Pages 140-151, ISSN 0038-092X, https://doi.org/10.1016/j.solener.2013.07.005.

[12] R. Pan, J. Kuitche and G. Tamizhmani, "Degradation analysis of solar photovoltaic modules: Influence of environmental factor," 2011 Proceedings - Annual Reliability and Maintainability Symposium, 2011, pp. 1-5, doi: 10.1109/RAMS.2011.5754514.

[13] Li, Heng-Yu. (2017). Assessment of Photovoltaic Module Failures in the Field. IEA report.

[14] Web resource: Manage risks and maximize ROI for your PV and energy storage projects (sinovoltaics.com)

[15] B. F. Nehme, T. K. Akiki, A. Naamane and N. K. M'Sirdi, "Real-Time Thermoelectrical Model of PV Panels for Degradation Assessment," in IEEE Journal of Photovoltaics, vol. 7, no. 5, pp. 1362-1375, Sept. 2017, doi: 10.1109/JPHOTOV.2017.2711430.

[16] Köntopp, M.B., Kröber, M., Schütze, M., & Taubitz, C. (2014). Potential Induced Degradation: Model Calculations and Correlation between Laboratory Tests and Outdoor Occurrence.

[17] P. Hacke et al., "Accelerated Testing and Modeling of Potential-Induced Degradation as a Function of Temperature and Relative Humidity," in IEEE Journal of Photovoltaics, vol. 5, no. 6, pp. 1549-1553, Nov. 2015, doi: 10.1109/JPHOTOV.2015.2466463.

[18] Mahmoud Dhimish, Violeta Holmes, Bruce Mehrdadi, Mark Dales, The impact of cracks on photovoltaic power performance, Journal of Science: Advanced Materials and Devices, Volume 2, Issue 2, 2017, Pages 199-209, ISSN 2468-2179, https://doi.org/10.1016/j.jsamd.2017.05.005.

[19] A. Bala Subramaniyan, R. Pan, J. Kuitche and G. TamizhMani, "Quantification of Environmental Effects on PV Module Degradation: A Physics-Based Data-Driven Modeling Method," in IEEE Journal of Photovoltaics, vol. 8, no. 5, pp. 1289-1296, Sept. 2018, doi: 10.1109/JPHOTOV.2018.2850527.

[20] Nick Bosco, Timothy J. Silverman, Sarah Kurtz, Climate specific thermomechanical fatigue of flat plate photovoltaic module solder joints, Microelectronics Reliability, Volume 62, 2016, Pages 124-129, ISSN 0026-2714, https://doi.org/10.1016/j.microrel.2016.03.024.

[21] Marc Köntges, Sarah Kurtz, Corinne Packard, Ulrike Jahn, Karl A. Berger, Kazuhiko Kato, Thomas Friesen, Haitao Liu, Mike Van Iseghem, Review of Failures of Photovoltaic Modules, IEA INTERNATIONAL ENERGY AGENCY, IEA-PVPS, ISBN 978-3-906042-16-9, March 2014

[22] Neha Bansal, Shiva Pujan Jaiswal, Gajendra Singh, Prolonged degradation and reliability assessment of installed modules operational for 10 years in 5 MW PV plant in hot semi-arid climate, Energy for Sustainable Development, Volume 68, 2022, Pages 373-389, ISSN 0973-0826, https://doi.org/10.1016/j.esd.2022.04.008.

[23] Y. R. Golive et al., "Analysis and Failure Modes of Highly Degraded PV Modules Inspected during the 2018 All India Survey of PV Module Reliability," 2020 4th IEEE Electron Devices Technology & Manufacturing Conference (EDTM), 2020, pp. 1-4, doi: 10.1109/EDTM47692.2020.9117930.

[24] Dhimish M, Alrashidi A. Photovoltaic Degradation Rate Affected by Different Weather Conditions: A Case Study Based on PV Systems in the UK and Australia. *Electronics*. 2020; 9(4):650. https://doi.org/10.3390/electronics9040650

[25] Köntges, Marc & Altmann, Sascha & Heimberg, Tobias & Jahn, Ulrike & Berger, Karl & Pvps, Iea. (2018). Mean Degradation Rates In Pv Systems For Various Kinds Of Pv Module Failures

Chapter 3

[1] Hoke, Anderson & Maksimovic, Dragan. (2013). Active power control of photovoltaic power systems. 2013 1st IEEE Conference on Technologies for Sustainability, SusTech 2013. 70-77. 10.1109/SusTech.2013.6617300.

[2] Rajan, Rijo & Fernandez, Francis. (2019). Power control strategy of photovoltaic plants for frequency regulation in a hybrid power system. International Journal of Electrical Power & Energy Systems. 110. 10.1016/j.ijepes.2019.03.009.

[3] Rijo Rajan, Francis M. Fernandez, Yongheng Yang, Primary frequency control techniques for large-scale PV-integrated power systems: A review, Renewable and Sustainable Energy Reviews, Volume 144, 2021, 110998, ISSN 1364-0321, https://doi.org/10.1016/j.rser.2021.110998.

[4] A. Sangwongwanich, Y. Yang and F. Blaabjerg, "High-Performance Constant Power Generation in Grid-Connected PV Systems," in IEEE Transactions on Power Electronics, vol. 31, no. 3, pp. 1822-1825, March 2016, doi: 10.1109/TPEL.2015.2465151.

[5] A. Sangwongwanich, Y. Yang, F. Blaabjerg and D. Sera, "Delta Power Control Strategy for Multistring Grid-Connected PV Inverters," in IEEE Transactions on Industry Applications, vol. 53, no. 4, pp. 3862-3870, July-Aug. 2017, doi: 10.1109/TIA.2017.2681044.

[6] V. A. K. Pappu, B. Chowdhury and R. Bhatt, "Implementing frequency regulation capability in a solar photovoltaic power plant," North American Power Symposium 2010, 2010, pp. 1-6, doi: 10.1109/NAPS.2010.5618965.

[7] Y. Kimpara, M. Kurimoto, Y. Manabe, T. Funabashi and T. Kato, "An Experimental Study on Active Power Control of Photovoltaic Power Generation for Supporting Grid Frequency Regulation," 2018 IEEE Power & Energy Society General Meeting (PESGM), 2018, pp. 1-5, doi: 10.1109/PESGM.2018.8586244

[8] Pankaj Verma, Tarlochan Kaur, Raminder Kaur, Power control strategy of an integrated PV system for active power reserve under dynamic operating conditions, Sustainable Energy Technologies and Assessments, Volume 45, 2021, 101066, ISSN 2213-1388, https://doi.org/10.1016/j.seta.2021.101066

Chapter 4

[1] M. Faifer, L. Cristaldi, S. Toscani, P. Soulantiantork and M. Rossi, "Iterative model-based Maximum Power Point Tracker for photovoltaic panels," 2015 IEEE

International Instrumentation and Measurement Technology Conference (I2MTC) Proceedings, 2015, pp. 1273-1278, doi: 10.1109/I2MTC.2015.7151456.

[2] Cristaldi, Loredana & Faifer, Marco & Laurano, Christian & Ottoboni, Roberto & Toscani, Sergio & Zanoni, Michele. (2020). Model-based maximum power point tracking for photovoltaic panels: parameters identification and training database collection. IET Renewable Power Generation. 14. 2876-2884. 10.1049/iet-rpg.2020.0101.

[3] P. Soulatiantork, L. Cristaldi, M. Faifer, C. Laurano, R. Ottoboni, S. Toscani, A tool for performance evaluation of MPPT algorithms for photovoltaic systems, Measurement, Volume 128, 2018, Pages 537-544, ISSN 0263-2241, https://doi.org/10.1016/j.measurement.2018.07.005.

[4] L. Cristaldi, M. Faifer, C. Laurano, R. Ottoboni, S. Toscani and M. Zanoni, "Model-Based MPPT Parameter optimization for Photovoltaic Panels," 2019 International Conference on Clean Electrical Power (ICCEP), 2019, pp. 534-538, doi: 10.1109/ICCEP.2019.8890100.

[5] L. Cristaldi, M. Faifer, C. Laurano, G. Leone and S. Toscani, "Model based Maximum Power Point Tracker stability over time," 2017 6th International Conference on Clean Electrical Power (ICCEP), 2017, pp. 591-595, doi: 10.1109/ICCEP.2017.8004748.

[6] COMMISSION REGULATION (EU) 2016/631 of 14 April 2016 establishing a network code on requirements for grid connection of generators [2016] OJ L 112

A. Appendix A

Arrhenius formula:

$$AF = A \cdot \exp\left(-\frac{E_a}{k_B \cdot T}\right) \tag{A-1}$$

AF acceleration factor

A constant

E_a activation energy

k_B Boltzmann constant

T temperature

Coffin Manson equation:

$$AF = \left(\frac{\Delta T_{test}}{\Delta T_{use}}\right)^n \tag{A-2}$$

AF acceleration factor

ΔT_{test} testing temperature variation

ΔT_{use} operating condition temperature variation

n fatigue factor

Norris Landberg equation:

$$AF = \left(\frac{f_f}{f_t}\right)^m \cdot \left(\frac{\Delta T_f}{\Delta T_t}\right)^{-n} \cdot \exp\left(\frac{E_a}{k_B}\left(\frac{1}{T_{m_f} - T_{m_t}}\right)\right) \tag{A-3}$$

AF acceleration factor

f cyclic frequency

ΔT temperature variation

E_a activation energy

k_B Boltzmann constant

T_{max} maximum temperature

Subscripts f: field, t: test

NOCT formula:

$$T_{mod} = T_{amb} + \frac{(NOCT - 20°C) \cdot G_m}{800 \frac{W}{m^2}} \tag{A-4}$$

T_{mod} module temperature

T_{amb} ambient temperature

NOCT Nominal Operating Cell Temperature

G_m module irradiation

Magnus formula:

$$RH_m = RH_{amb} \cdot e^{\left(\frac{17{,}62 \cdot T_{amb}}{243{,}12°C + T_{amb}}\right) - \left(\frac{17{,}62 \cdot T_{mod}}{243{,}12°C + T_{mod}}\right)} \tag{A-5}$$

RH_m module relative humidity

RH_{amb} ambient relative humidity

T_{amb} ambient temperature

T_{mod} module temperature

Peck equation:

$$AF = A \cdot \exp\left(-\frac{E_a}{k_B \cdot (T_f - T_t)}\right) \cdot RH\%^{-n} \tag{A-6}$$

AF acceleration factor

E_a activation energy

k_B Boltzmann constant

T temperature

$RH\%$ percentual relative humidity

n constant

Subscripts f: field, t: test

List of Figures

List of Tables

2. List of Symbols

Variable	Description	SI unit
$\boldsymbol{E_a}$	Activation energy	eV
$\boldsymbol{k_B}$	Boltzmann constant	eV/K
$\boldsymbol{G}$	Irradiation	W/m^2
$\boldsymbol{I}$	Current	A
$\boldsymbol{P}$	Power	W
$\boldsymbol{R}$	Resistance	Ω
$\boldsymbol{RH}$	Relative humidity	%
$\boldsymbol{T}$	Temperature	K
$\boldsymbol{V}$	Voltage	V
$\boldsymbol{f}$	Frequency	Hz
$\boldsymbol{t}$	Time	s
$\boldsymbol{R}$	Gas constant	$J/K \cdot mol$

3. Acknowledgements

I would like to give my warmest thanks to my supervisor Prof. Loredana Cristaldi for helping me with this work, for her guidance and her patience. I would also like to express my sincere thanks to Dr. Christian Laurano and PhD. Emil Petkovski for their precious suggestions and encouragements. Finally, I would like to thank my family and my friends for their support during these years.